Investigations of the exchange energy of neutral atoms in the large-Z limit

Jeremy J. Redd
Department of Physics, Utah Valley University, Orem, UT 84058, USA

Antonio C. Cancio
Department of Physics and Astronomy, Ball State University, Muncie, IN 47306, USA; accancio@bsu.edu

Nathan Argaman
Department of Physics, Ben-Gurion University, Beer-Sheva 84105, Israel; Department of Physics,
Nuclear Research Center—Negev, P.O. Box 9001, Be'er Sheva 84190, Israel

Kieron Burke
Departments of Physics and Astronomy and of Chemistry,
University of California, Irvine, CA 92697, USA
(Dated: Monday 9th October, 2023)

The non-relativistic large-Z expansion of the exchange energy of neutral atoms provides an important input to modern non-empirical density functional approximations. Recent works report results of fitting the terms beyond the dominant term, given by the local density approximation (LDA), leading to an anomalous $Z\ln Z$ term that can not be predicted from naive scaling arguments. Here, we provide much more detailed data analysis of the mostly smooth asymptotic trend describing the difference between exact and LDA exchange energy, the nature of oscillations across rows of the periodic table, and the behavior of the LDA contribution itself. Special emphasis is given to the successes and difficulties in reproducing the exchange energy and its asymptotics with existing density functional approximations.

1. INTRODUCTION

Almost a century of painstaking physical and mathematical work has proven that the asymptotic expansion of the non-relativistic energy of the neutral atom is

$$E \to -c_0 Z^{7/3} + Z^2/2 - c_1 Z^{5/3} + ... \quad (Z \to \infty), \quad (1)$$

where Z is the nuclear charge (in Hartree atomic units)[1]. Remarkably, the simplest density functional approximation, that of Thomas-Fermi theory[2, 3], yields precisely the leading term, allowing c_0 to be calculated to arbitrary accuracy from the solution of the Thomas-Fermi differential equation for neutral atoms[4]. In fact, Lieb and Simon proved that Thomas-Fermi theory becomes relatively exact for the total energy of any electronic system in a carefully defined semiclassical limit[5, 6].

Modern electronic structure calculations are dominated by Kohn-Sham density functional theory[7], in which only the exchange-correlation energy, E_{xc}, need be approximated as a functional of the density. It has been conjectured (and proven under various assumptions) that, in the same limit, $E_{\mathrm{xc}}^{\mathrm{LDA}}$ becomes relatively exact[1, 8–14]. For exchange alone,

$$E_{\mathrm{x}} \to -d_0 Z^{5/3} + ...(Z \to \infty), \quad (2)$$

where $d_0 = 9c_1/11$ and is given exactly by the local density approximation (LDA) for exchange (given by the Dirac model[15]), applied to the TF density[4]. It has further been found numerically that several popular generalized gradient approximations (GGAs) are quantitatively accurate for the leading correction to LDA.[10] The construction of several approximate semilocal functionals, including
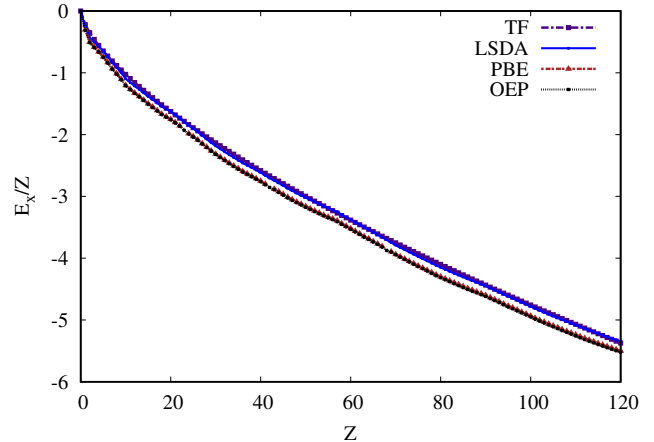
FIG. 1. Exchange energy per electron versus nuclear charge Z for neutral atoms up to $Z = 120$, exactly (black), within LDA(blue),and with PBE (red). The leading order term in the large-Z expansion, Dirac exchange applied to the TF density, is shown with violet dot-dashed line.

PBEsol[16], SCAN[17], and acGGA[13], have incorporated these insights. Unfortunately, even the analytic form of these leading corrections is unknown. Kunz and Rueedi [11] have discussed possible higher-order terms in the asymptotic expansion for exchange, distinguishing between a series with a smooth dependence on Z, and oscillating terms which appear in higher orders.[18] They argue the need for smooth corrections to the leading order term in Eq. 2 of order $Z^{4/3}$ and $Z\ln Z$ terms but did not calculate the associated coefficients or provide a proof for their existence.

Fig. 1 illustrates just how devilishly difficult it can be to find these leading corrections. The figure shows exchange energy per electron as a function of Z. It includes the simple asymptotic behavior, the local density approximation (LDA) and a popular GGA, as well as highly accurate energies from OEP calculations. Hidden in these barely distinguishable lines are all the shell structure of the periodic table, and very subtle trends in the differences. On this scale, the leading order term of the expansion, derivable from the primitive TF-Dirac model for exchange does quite well, and all the complications of modern functionals only amount to a small perturbation. This illustrates the challenge of the task of extracting accurate and correct asymptotic behaviors, when even the form to be used is uncertain.

Nevertheless, there have been a number of attempts to elucidate the form and coefficients by careful numerical analysis of the available data. The quantity $\Delta E_{\mathrm{x}} = E_{\mathrm{x}} - E_{\mathrm{x}}^{\mathrm{LDA}}$ is much smoother and so simpler to model than E_{x} itself. Original works of this sort [10, 19] used an overly simple model based on a naive scaling analysis of the gradient expansion correction to LDA that neglected changes in the density as a function of Z. This assumes that the form of the leading correction to ΔE_{x} was in simple powers of $Z^{1/3}$, neglecting the possibility of non-analytic contributions. In the range of Z between 10 and 56 and with only noble gas atoms, this fit is indeed quite reasonable numerically.

Recent work [20–22] has revealed a flaw in this approach. The gradient expansion correction to the LDA energy diverges on the TF density. Correction of the TF density near the nucleus leads to a leading order term of $Z\ln Z$. Based on this insight, recent work [21] revisited exchange data for atoms, this time up to $Z = 120$, finding a remarkably efficient fit of ΔE_{x} of closed shell atoms to the form $-Z(B\ln Z + C)$. The leading coefficient is several times larger than that predicted by the gradient expansion of exchange[23] applied to this system. The fit matches atomic exchange energies down to $Z = 1$, and the coefficients are independent of fit range and details. An explanation for this result comes from analysis of the Bohr atom[24], consisting of noninteracting electrons in a Coulomb potential. This analysis both validates the need for a $Z\ln Z$ term and provides an explanation for the ratio of the numerically observed B coefficient to that of the gradient expansion.[21, 22]

The older results have been used in the construction of several recent approximate functionals. Such fits yield accurate results for the limited range of the fit, and hence approximations trained on such fits are accurate for large Z atoms. But the new analysis complicates the picture, especially as two coefficients are now needed to acheive the same accuracy. The complicated behavior of the density as a function of Z makes the relationship between semilocal functionals of the density complicated, with density functional errors harder to diagnose and fix. It also leads to a complicated expansion picture for LDA exchange, with many terms beyond the $Z^{5/3}$ term characterizing the asymptotic limit, and oscillations as a function of the fractional filling of rows of the periodic table.

The present work presents a detailed study of both the oscillatory $E_{\mathrm{x}}^{\mathrm{LDA}}(Z)$ data and the much smoother $\Delta E_{\mathrm{x}}(z)$ results, with special attention given to the successes and difficulties in reproducing the exchange energy and its asymptotics with existing density functional approximations.

Organization of the rest of this paper is as follows: Sec. 2 presents background of our study, including an overview of the asymptotic expansion of exchange of atoms and an analysis of the gradient expansion, including higher order terms. Sec. 3 briefly reviews numerical methods, Sec. 4 presents a comparison of the beyond-LDA contribution ΔE_{x} for exact exchange and common GGA functionals, Sec. 5 presents our results for LDA exchange, and finally, Sec. 6 presents outcomes and conclusions.

2. BACKGROUND

The connection between asymptotic expansions and modern density functionals for exchange-correlation was first discussed in Ref [19], with the appropriate formalism illustrated for the one-dimensional kinetic energy in Ref [25]. The key analytic insight is provided by the scaling procedure of the TF model, expressed in theorems developed by Lieb and Simon. [5, 6] The Lieb-Simon limit is approached by simultaneously scaling the potential by a factor ζ tending to ∞ and changing the particle number. For any potential $v(\mathbf{r})$, define a ζ-scaled potential $v_\zeta(\mathbf{r}) = \zeta^{4/3} v(\zeta^{1/3}\mathbf{r})$, and simultaneously replace N, the electron number, with ζN, choosing ζ so the latter remains an integer. This applies to all atoms, molecules, and solids. For any finite interacting electronic system, the expansion will have the same form as Eq. 1, but with different, system-dependent coefficients. Because N changes, this can be a challenging limit to study in practice, and almost all numerics for interacting systems have been extracted solely in the simple case of neutral atoms, where ζ-scaling is equivalent to changing Z, keeping $N = Z$. The Lieb-Simon theorem states that, for any electronic system, TF theory yields the leading order term (the $Z^{7/3}$ contribution) exactly.

For atoms, Schwinger first showed[8] in convincing detail that LDA exchange yields precisely the dominant term, with many further details extracted with Englert[26, 27]. Later, Conlon [9], followed up with greater mathematical rigor by Fefferman and Seco[28] gave a general proof for arbitrary systems.

Beyond the leading order term, however, little is known for certain, even the form of the large-Z expansion for the exchange energy. Kunz and Rueedi[11] found success for 2D quantum dots considered as artificial atoms, but crucially, these lack the complicating factor of the singular Coulomb potential. We take their conjecture that the large-Z expansion of the exchange energy of atoms has at its basis a form that is a smooth function of Z:

$$E_{\mathrm{x}}(Z) \to -\left(d_1 Z^{5/3} + A_{\mathrm{x}} Z^{4/3} + Z(B_{\mathrm{x}}\ln Z + C_{\mathrm{x}})\right) + \cdots$$
$$(3)$$

as $Z \to \infty$. However these coefficients are expected to
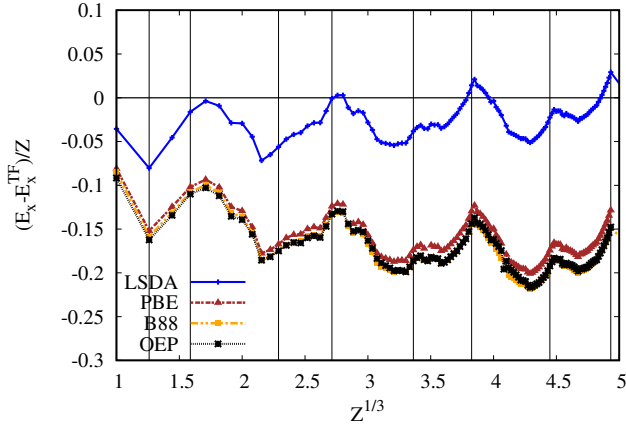
FIG. 2. Asymptotic residual of exchange. Shows what is left over of the exchange energy/particle when the leading term in the asymptotic expansion for exchange $-(9/11)0.2699Z^{2/3}$ is removed. Shown is the OEP data from opmks, the LDA, B88 exchange, PBE, and an asymptotically corrected PBE from Ref. 12 that might be deleted. The line at zero gives the Thomas-Fermi limit of the exchange energy. The vertical lines shows the location of each atom with a filled s^2 valence shell (He and the alkali earths.)

vary with each column of the periodic table, leading to oscillations in energy across each row of the table. Thus, for an accurate description of the exchange energy of every atom, the smooth form must be augmented by an oscillatory piece, expressed (at least in part) in terms of coefficients that depend on the fraction of filled shells.[1, 18] This is straightforward in the case of the kinetic energy of Bohr atoms[1, 12], but is much more complex for the real periodic table. Fortunately, as we show below, and as discussed in Refs. 10, 20, and 21, these oscillations are to a large degree not relevant to density functional development.

Now define the beyond-asymptotic exchange energy for each Z as:

$$E_{\mathrm{x}}^{\mathrm{BA}}(Z) = E_{\mathrm{x}}(Z) + d_1 Z^{5/3}, \qquad (4)$$

so that for large Z, ignoring oscillatory effects,

$$\frac{E_{\mathrm{x}}^{\mathrm{BA}}(Z)}{Z} \to -\left(A_{\mathrm{x}} Z^{1/3} + B_{\mathrm{x}}\ln Z + C_{\mathrm{x}}\right) + \cdots. \qquad (5)$$

Figure 2 shows $E_{\mathrm{x}}^{\mathrm{BA}}(Z)$ exactly and for various approximations. Already, the simple subtraction of the leading asymptotic contribution highlights the differences and makes the periodic structure visible. It also illustrates a relatively slow average variation with $Z^{1/3}$.

LDA has oscillations strongly correlated with those seen in exact exchange but a significantly different smooth contribution. Removing this contribution from the asymptotic expansion removes much of the complications of this periodic structure while retaining the target of beyond-LDA density functional models of exchange. Thus, assuming the same qualitative behavior, we define the local beyond-asymptotic
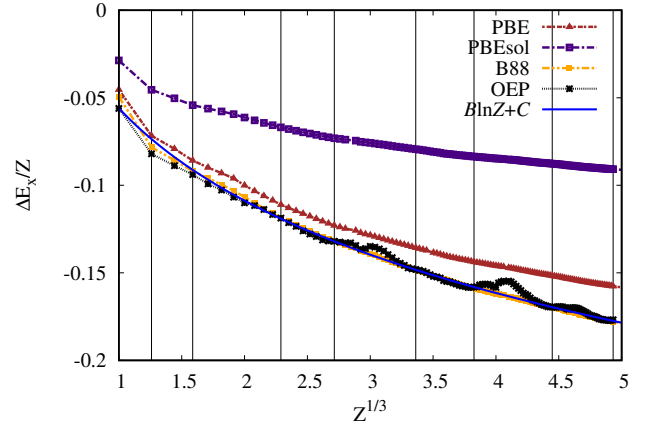
FIG. 3. Difference with LDA or beyond-LDA exchange energy per electron. The details are the same as the previous two figures.

(LBA) energy as

$$E_{\mathrm{x}}^{\mathrm{LBA}}(Z) = E_{\mathrm{x}}^{\mathrm{LDA}}(Z) + d_1 Z^{5/3}, \qquad (6)$$

with a smooth large-Z expansion of

$$\frac{E_{\mathrm{x}}^{\mathrm{LBA}}(Z)}{Z} \to -\left(A_{\mathrm{x}}^{\mathrm{LDA}} Z^{1/3} + B_{\mathrm{x}}^{\mathrm{LDA}}\ln Z + C_{\mathrm{x}}^{\mathrm{LDA}}\right) + \cdots, \qquad (7)$$

as LDA surely also yields the correct leading asymptotic term. Their difference $\Delta E_{\mathrm{x}}(Z) = E_{\mathrm{x}}(Z) - E_{\mathrm{x}}^{\mathrm{LBA}}(Z)$, the beyond-local contribution to exchange, has an expansion

$$\frac{\Delta E_{\mathrm{x}}(Z)}{Z} \to -\left(\Delta A_{\mathrm{x}} Z^{1/3} + \Delta B_{\mathrm{x}}\ln Z + \Delta C_{\mathrm{x}}\right) + \cdots. \qquad (8)$$

for large Z. Here, then, $\Delta A_{\mathrm{x}} = A_{\mathrm{x}} - A_{\mathrm{x}}^{\mathrm{LDA}}$, etc. Figure 3 shows the difference between LDA and exact energies, and is clearly far smoother than Fig. 2. As plotted, $\Delta E_{\mathrm{x}}/Z$ has a form $\Delta A Z^{1/3} + \Delta B\ln Z + \Delta C$ that lends itself to visual analysis, and it is apparent that the trend is much more likely that of a log curve, than, for example, a straigbt line. As noted by Elliot and Burke in their original work[10], the approximate exchange energies of PBE[29] and of Becke 88 (B88)[30], the exchange component of BLYP, follow very closely the smooth asymptotic trend of the exact data. (Unfortunately, they plotted data versus $Z^{-1/3}$, and not $Z^{1/3}$, a a strategy optimized for extracting asymptotic coefficients, but obscuring the trend in the asymptotic form.) A third density functional, PBEsol,[16] is also shown as a proxy for the second-order gradient expansion which it approaches for a system with a slowly varying density. The plot shows clearly the underestimate of the gradient expansion of the beyond-LDA exchange as compared to OEP, and the much better reproduction of this data achieved by PBE and B88 by breaking this constraint.

Fig. 4 confirms the logarithmic behavior of the leading order term of $\Delta E_{\mathrm{x}}/Z$. It shows the results of fits assuming leading order terms in $\Delta E_{\mathrm{x}}/Z$ to be $Z^{1/3}$ (brown),
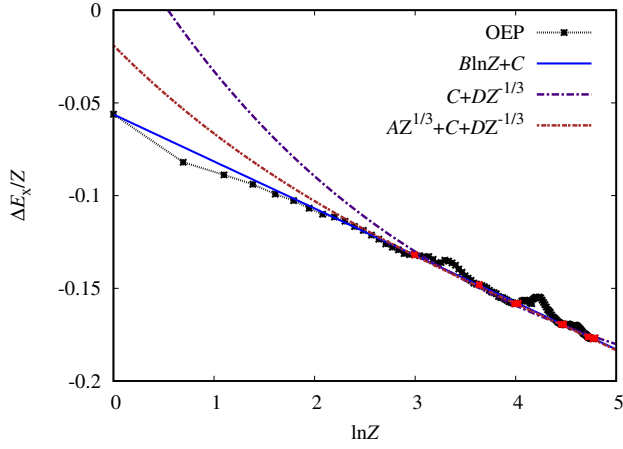
FIG. 4. Beyond-LDA exchange energies per electron. OEP is optimized effective potential, the other three curves are fits to various asymptotic models as described in the text. OEP data used to make the fits are highlighted in red.

$\ln Z$ (blue) or constant (violet), or leading order coefficients of ΔA_x, ΔB_x or ΔC_x respectively, plotted versus $\ln Z$. Each fit is on a set of closed-shell atoms highlighted in red on the figure; they are described in Ref. 21 and partly shown in Fig. 1 of the same. The fits are all reasonably close to data within the range of Z values, $\ln Z \geq 3$, of the fit set. However, only the logarithmic model has predictive power outside this range – in fact extrapolating almost exactly down to $Z = 1$. It is not surprising that varying the fit set of atoms (including using all the data) yields no statistically significant change in this fit. We are thus confident that an expression for ΔE_x of the form

$$\Delta E_\mathrm{x}^{fit} \to -(\Delta B_\mathrm{x} Z \ln Z + \Delta C_\mathrm{x} Z) \tag{9}$$

gives an accurate description of exact exchange for the data available.

2.1. Application to KS DFT

In KS DFT, we are required to give E_x as a functional of the density. As ζ becomes large, the exchange functional approaches the local density approximation:

$$E_\mathrm{x}[n_\zeta] \to \int d^3r \, e_\mathrm{x}^{\mathrm{LDA}}(n_\zeta(\mathbf{r})) = -c_\mathrm{x} \int d^3r \, n_\zeta(\mathbf{r})^{4/3}, \tag{10}$$

where $c_\mathrm{x} = (3/4)(3/\pi)^{1/3}$. As the density also weakly approaches the TF density, evaluation on that density yields the coefficient d_1 in Eq. 2 [4]. Next, we equate $\Delta E_\mathrm{x}(Z)$ defined in Eq. (8) with the difference between the LDA and exact exchange functional

$$\Delta E_\mathrm{x}(Z) = E_\mathrm{x}[n_Z] - E_\mathrm{x}^{\mathrm{LDA}}[n_Z^{\mathrm{LDA}}], \tag{11}$$

where n_Z is the exact KS density for the Z electron system and n_Z^{LDA} the LDA density for the same. This formulation

may be extended to approximate exchange functionals. Almost all those in modern use (including all those discussed here) recover LDA in the uniform (or large-Z) limit, so that $\Delta E_\mathrm{x}/E_\mathrm{x} \to 0$ as $s^2 \to 0$.

2.1.1. Gradient expansion

The natural next step beyond the local density approximation is the gradient expansion. For a slowly-varying (infinitely extended) electron gas, this is the expansion of its energy in increasing (higher-order) gradients of the density. This expansion is well-defined, and is likely asymptotic when applied to any gas of slow but finite variation[31]. The application of this expansion to finite systems as an approximate density functional is called the gradient expansion approximation, GEA.

For atoms, most of the density becomes slowly varying in the LS limit, i.e., the local dimensionless gradient vanishes as the limit is approached. But the region near the nucleus and the vicinity of the evanescent region, do not. As the nucleus is approached, the GEA produces an anomalous contribution to kinetic energy of order Z^2 (but not the correct -1/2 coefficient)[4] For exchange, as we show below, GEA produces an anomalous $Z \ln Z$ term, suggesting that such a term might be present in the exact functional. Moreover, modern semilocal approximations can be expanded in the slowly-varying limit, although many do not recover the correct coefficient for the slowly-varying gas. Thus both the exact and most approximate functionals can be expected to manifest this logarithmic behavior for exchange for large Z.

For exchange, we write the gradient expansion in terms of second-order $\Delta E_\mathrm{x}^{(2)}$ and fourth order $\Delta E_\mathrm{x}^{(4)}$ terms as

$$E_\mathrm{x}^{\mathrm{GE}} = E_\mathrm{x}^{\mathrm{LDA}} + \Delta E_\mathrm{x}^{(2)} + \Delta E_\mathrm{x}^{(4)} + \cdots. \tag{12}$$

The second-order gradient correction is of most importance here and is given by

$$\Delta E_\mathrm{x}^{(2)} = \mu_2 \int s^2 e_\mathrm{x}^{\mathrm{LDA}}(n(\mathbf{r}))d^3r \tag{13}$$

with $\mu_2 = 10/81$ [23] and s^2 is a scale-invariant gradient given by

$$s^2 = \frac{|\nabla n|^2}{4k_F^2 n^2} \tag{14}$$

where $k_\mathrm{F} = (3\pi^2 n)^{1/3}$ is the local Fermi wavevector. To generate the leading beyond-LDA term in the exchange expansion, one can first try a naive scaling argument. Apply the second-order gradient expansion to the TF density $n^{\mathrm{TF}}(\mathbf{r})$. Note [4] that for any finite value of r, $s^2 \sim Z^{-2/3}$ for the TF density, while the LDA gives a factor of $Z^{5/3}$. The end result of Eq. 13 should give the order of the first term beyond leading order, and is of order Z.

To obtain a logarithmic term from the gradient requires more careful analysis of the contribution from the very high

density inner core of the large-Z atom.[21] Here, $n^{\text{TF}}(r)$ diverges as $1/x^3$ and s^2 diverges as $1/x$, where $x = Z^{1/3}r/a$ is the scaled distance derived from TF theory[1], and $a = (1/2)(3\pi/4)^{2/3}$. Thomas-Fermi theory breaks down for $s^2 \sim 1$ and care must be taken to ensure finite integrals. Including the divergence of the TF density at the nucleus produces divergent integrals. For the region inside $x \sim 1$, the location of the peak of the radial density probability, we have

$$n(r) \sim \frac{Z^2}{4\pi a^3} x^{-3/2} \qquad (15)$$

$$e_{\text{x}}^{\text{LDA}} d^3 r \sim Z^{5/3} \frac{c_{\text{x}}}{(4\pi)^{1/3}} dx \qquad (16)$$

$$s^2 \sim \frac{a_1^2}{Z^{2/3}} x^{-1} \qquad (17)$$

where $a_1 = (1/2)(9/2\pi)^{2/3}$ [4]. With the resulting integrand diverging as $1/x$ as $x \to 0$, $\Delta E_{\text{x}}^{(2)}$ diverges logarithmically. The natural small-radius cutoff is $r \sim 1/Z$, the distance from the nucleus in units of a_B inside which TF theory fails. This translates to $x \sim Z^{-2/3}$ so we find a net contribution to the leading order of

$$\Delta E_{\text{x}}^{(2)} \sim \int_{Z^{-2/3}}^{1} x^{-1} dx = \frac{2}{3} Z \ln Z + \mathcal{O}(Z). \qquad (18)$$

Restoring constants produces

$$\Delta E_{\text{x}}^{(2)} \sim \Delta B_2^{\text{GEA}} Z \ln Z + \Delta C_2^{\text{GEA}} Z, \qquad Z \to \infty \qquad (19)$$

with

$$\Delta B^{\text{GEA}} = \frac{3}{4\pi^2} \mu_2. \qquad (20)$$

To see if higher orders in the gradient expansion alter this coefficient, we proceed with the fourth-order contribution in a similar fashion. The general form is

$$\Delta E_{\text{x}}^{(4)} = \int (\mu_{pp} p^2 + \mu_{pq} pq + \mu_{qq} q^2) e_{\text{x}}^{\text{LDA}} d^3 r, \qquad (21)$$

where the μ's are known coefficients. Here, $p = s^2$ and $q = \nabla^2 n / 4k_F^2 n$ is the scale-invariant Laplacian of the density. Since $q = p/3$ for the region of space where the logarithmic divergence in $\Delta E_{\text{x}}^{(2)}$ occurs,[4] we find

$$\Delta E_{\text{x}}^{(4)} \sim \mu_4 \int d^3 r p^2 e_{\text{x}}^{\text{LDA}}, \qquad (22)$$

where $\mu_4 = \mu_{pp} + \mu_{qp}/3 + \mu_{qq}/9$. An analysis similar to that for 2nd-order shows that the integral scales naively as $Z^{1/3}$, but the integrand varies as $1/x^2$. The overall behavior is

$$\Delta E_{\text{x}}^{(4)} \sim Z^{1/3} \int_{Z^{-2/3} x_1}^{x_2} x^{-2} dx \sim Z/x_1 \qquad (23)$$

In this case we can't eliminate a constant x_1 that determines the exact small-radius cutoff, but a good criterion

for this can be found, as we show below. More important is to note that neither the fourth-order GE, nor any high-order order term in the gradient expansion contributes to the logarithmic contribution ΔB_{x} to ΔE_{x}: it only comes only from the second-order gradient expansion as far as we can tell.

Thus, the minimal density functional approximation that captures the leading order term in exchange beyond the LDA is the GGA, which has the general formulation given by

$$E_{\text{x}}^{\text{GGA}} = \int d^3 r F_{\text{x}}(s^2) e_{\text{x}}^{\text{LDA}}, \qquad (24)$$

which typically reduces to the form of the second-order gradient expansion, $F_{\text{x}} \sim 1 + \mu s^2$, in the slowly-varying limit, $s^2 \to 0$. As we show in Sec. 4.4, meta-GGAs only add significant corrections to this form to fourth-order and are less relevant here. Different GGA's produce different ΔB_{x} coefficients because of differing values for μ. Thus the PBEsol [16] uses the gradient expansion coefficient, $\mu = 10/81 \sim 0.123$, but PBE [29] has $\mu = \beta\pi^2/3 \sim 0.21951$ based on a different choice of constraints, and B88 [30], has $\mu = 0.275$. But our asymptotic model [Eq. (19)] of actual atom exchange energies has $\mu \sim 1/3$, considerably larger than all these.

This discrepancy indicates the limitation (first pointed out in Ref. 19) of the gradient expansion as a model for Coulombic systems. The gradient expansion is derived for slowly-varying gases, without classical turning points at the Fermi level – something that is not true for any atom with finite Z. In addition to the Coulomb singularity that ensures there will be a finite region near the nucleus where Thomas-Fermi analysis fails, the classical turning point at the valence edge necessarily requires corrections of fundamentally different form than the gradient expansion, as discussed in Ref. [32]. Indeed, the Scott term in the total energy[33], of order Z^2 [Eq. (1)], is evidence of such corrections. More precisely, a term $\sim Z^2$ is generated from the gradient expansion for the total energy by using an analysis of the inner core equivalent to that discussed here for exchange, but the coefficient has the wrong sign and magnitude. The correct coefficient of -1/2 is easily deduced by the direct analysis of the Bohr atom however.[12] It seems likely, therefore, that the same thing is happening for exchange: the gradient expansion indicates the need for an anomalous $Z \ln Z$ term but does not determine the correct coefficient.

Based on this insight, Ref. 21 applied an analysis of the exchange energy of the Bohr atom to find that the exact exchange indeed had a logarithmic $Z \ln Z$ term, with a coefficient that was exactly 2.7 times the value obtained by the GEA applied to that system. Assuming that the same ratio should hold for real atoms, yields a correction of $2.7 \Delta B^{\text{GEA}}$ [Eq. (20)] or $1/4\pi^2$. Further requiring, with probably somewhat less reasonability, that $Z = 1$ should yield the exact E_{x} for hydrogen produces the following conjecture for the beyond-local contribution: '

$$\Delta E_{\text{x}} = -Z \left(\ln Z / (4\pi^2) + 5/16 - 0.2564 \right). \qquad (25)$$

This remarkably matches our numerical parameters within their statistical error.

3. METHODS AND NUMERICAL CHECKS

In the following we must distinguish between trends with Z, $Z \log Z$ and $Z^{4/3}$. To do so, we extend our data set to as high a Z as possible, ignoring issues of experimental stability and relativity, a task that involves two different atomic DFT codes. First we use the optimized effective potential code opmks [34] to perform nonrelativistic exact exchange and spin-density dependent, self-consistent density functional calculations for all neutral atoms up to $Z = 120$. Unfortunately, the inversion problem used to find the potential in the OEP begins to fail for $Z > 120$ and DFT calculations using OPMKS fail to converge reliably for $Z > 362$.

For GGAs and the LSDA for large-Z atoms ($Z > 120$) we use the atomic pseudopotential code FHI98PP[35] in its all-electron, non-relativistic mode. This code enables us to make GGA and LDA calculations extending the periodic table to $Z = 978$ without significant sign of numerical stress. This corresponds to 16 full shells of the periodic table, and one filled 17s shell – the alkali earth metal with valence shell 17s^2. (A few atoms had frontier orbitals that failed to converge properly, mostly open-shell atoms and two closed-shell atoms of the extended periodic table with frontier orbitals with a high angular momentum.)

FHI98PP computes wavefunctions on a grid of radial points, with spacing between successive points increasing by a geometric factor γ. We use the default grid which starts at $r = 0.00625/Z$, with a step size that increments by a growth factor $\gamma = 1.0247$ out to a maximum radius of 80. To check the quality of FHI98PP energies, the highest occupied orbital energy eigenvalues were compared to those of OPMKS for closed shell atoms with $Z < 362$ using LSDA exchange. These calculations were done both using a finer and more course grid than the default. The results are indistinguishable within machine precision. The details of the stress test can be seen in the supplementary materials.

The shell structure of the large-Z atoms was assumed to follow the Madelung principle for closed shell atoms. The validity of this extension has been tested by comparing the total energy of Aufbau-constructed shells versus several other shell configurations for elements 976 (filled 16p), 970 (filled 15d), and 816 (filled 16s). For all cases tested, the Aufbau construction yields the nonrelativistic ground state for these atoms.

An important potential source of error is the use of OEP to obtain exact exchange energies – the true ground state has correlation energy, which will slightly change the density and orbitals used to evaluate exchange. We do not have a way to assess this issue directly. However, as a proxy, we have calculated beyond-local exchange energies using the difference between OEP and LDAX (i.e. using LDA exchange only), on the principle that this should cancel some of the error of not treating correlation in the OEP. Refitting

the coefficient ΔB_x for the leading beyond-local term in exchange leads to a value of 0.0248, a 2% change in the fitted value of 0.0254 reported in Ref. 21. A similar calculation, comparing OEP with PBE correlation to LSDA, yields 0.0250. These results are an order of magnitude smaller an effect than the discrepancies we see between the predictions for this quantity by GGA and our model, and is nearly within statistical error.

Statistical fits used gnuplot plotting and Levenberg-Marquardt nonlinear regression. A list of approximate and exact exchange energies used in this paper is included in the supplementary materials.

4. RESULTS WITH APPROXIMATE FUNCTIONALS

4.1. Generalized gradient approximations

How do standard DFT approximations perform in reproducing the asymptotic behavior of exact exchange data? To find out, we recast our data so as to extract efficiently the asymptotic character of the exchange energy. Starting with the asymptotic form $\Delta E_\mathrm{x}^{asy}$ [Eq. (9)] describing the nonoscillatory contribution to the beyond-LDA exchange energy in the large Z limit, we reframe it as

$$\frac{\Delta E_\mathrm{x}^{asy}}{Z \ln Z} = \Delta B_\mathrm{x} + \Delta C_\mathrm{x} x, \qquad (26)$$

where $x = 1/\ln Z$. Plotting $\Delta E_\mathrm{x}^{asy}/Z \ln Z$ versus x casts this relation as a straight line with y-intercept ΔB_x and slope ΔC_x. This plotting convention yields an easy visual comparison to the behavior of exact exchange and of approximate functionals. Fig. 5 shows the results. Black crosses show the beyond-LDA exchange energy for OEP, and the black line extrapolating to $x = 0$ is the asymptotic model Eq. 25, with the y-axis intercept shown as a green circle. We place vertical lines at the location on the x axis of the alkali earth atoms, from 8s^2 ($Z = 120$ or $x = 0.21$) to 2s^2 ($Z = 4$, $x = 0.72$). Helium and hydrogen have $x > 1$ and are not shown.

Similar plots are included on the figure for three different GGA's: PBEsol, PBE, and BLYP, each evaluated on an extended data set including closed shell atoms up to $Z = 978$. The asymptotic trend to large Z for each is estimated by taking a linear fit for $x < 0.18$ ($Z \geq 260$) and extrapolating to $x = 0$ and shown as a straight line. As discussed in Sec. 3, the theoretical large-Z limit of a GGA is determined by the its coefficient μ, yielding a prediction for B [Eq. (20)] proportional to μ. The prediction for each GGA is shown as an additional green circle on the y-axis.

We do not compare directly to the gradient expansion because of the large errors it suffers in the exponential tail of small atoms (where s^2 diverges to infinity). Instead we use PBEsol as a surrogate, as it yields the exact second-order gradient expansion ($\mu = 10/81$) for the slowly-varying gas. PBEsol mimics the general trend of the OEP correctly, i.e., it has a reasonably close slope or ΔC_x coefficient. But
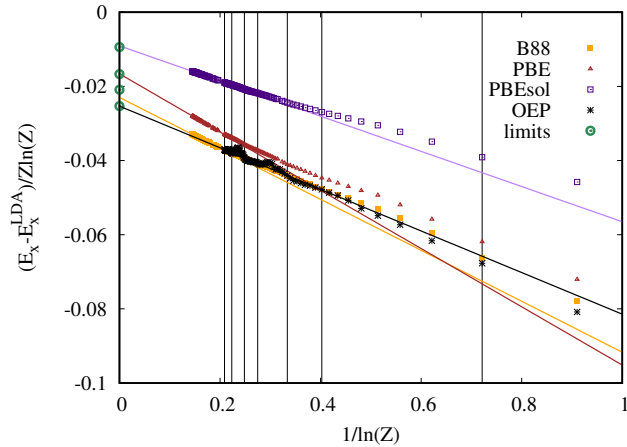
FIG. 5. Extrapolation of beyond-LDA exchange energies per electron to the $Z \to \infty$ limit for OEP data and several common GGA's. The y-axis intercept yields the coefficient ΔB_{x}. PBEsol is included as a proxy for the gradient expansion. Black line is the semi-theoretical result of Ref. [21] while the other straight lines are fit to DFT models for $Z > 259$. Green dots are calculated theoretical limits of each model and the OEP.

FIG. 6. Extrapolation of difference between DFT exchange energies-per-particle and our smooth asymptotic model to the $Z \to \infty$ limit. acPBE has a gradient expansion coefficient of $\mu = 0.2605$ as suggested by Ref. 10. Theoretical values for extrapolated ΔB_{x} coefficients shown as green dots and fits to functionals as straight black lines. Location of alkali earths indicated by vertical black lines as guide to the eye.

its intercept is nearly one-third too small, consistent with the finding in Sec. 2. This leads to a significant error in exchange energies of atoms.

At the same time, by roughly doubling μ compared to the gradient expansion, PBE and BLYP correct for the PBEsol errors for Z of chemical relevance but still fall short of reaching the predicted ΔB_{x} from asymptotic analyis. The extrapolated large-Z behavior of each density functional, with the notable exception of BLYP, is close to that obtained from the coefficient of the second-order gradient expansion of each model. This corroborates the assessment in Sec. 2 that the value of ΔB_{x} obtained in a gradient expansion is determined from the second-order contribution only, [Eq. (20)], and not from higher-orders. As we shall see below, even B88, the exchange functional of BLYP, can be made to comply with a little extra work.

4.2. Asymptotic analysis of remainder

We performed one further piece of analysis, to plot the difference between the exchange energy-per-particle of several approximations and the "nearly" theoretical model of Eq. (25). This is shown for the OEP and several GGA approximations to the exchange energy in Fig. 6 using the same convention for x and y axes as Fig. 5.

At the fine energy scale revealed by subtracting off the leading order terms to the beyond-LDA expansion, the small oscillations in the OEP data becomes significant.

The figure shows that our theoretical model for the asymptotic limit has, to some extent, captured the trend of the lower energy edge of the oscillations in OEP. The upper peaks occur at filled 2p, 3d, 4f valence shells (Ne, Zn,

Yb), and trend to a rather different asymptote. (To identify Ne, note that the bars show filled alkali earths, starting with the $8s^2$ filled valence shell and working back to $2s^2$. Ne is the peak two atoms from Mg, the vertical line at $x \sim 0.4$). The amplitude of oscillation is roughly 0.003 $Z\ln Z$ ($3Z\ln Z$ in mHa) in the range of Z values for which we have data, i.e. an order of magnitude lower than the $Z\ln Z$ coefficient for the smooth asymptotic trend. It is also quite possible that these oscillations grow as $Z^{4/3}$, as do those of the total energy [1] and, as we shall show presently, those of the LDA exchange energy of real atoms. In comparison, the GGA's greatly underestimate the magnitude of these oscillations, although it seems that they do have small "kinks" at roughly the same Z values as the minima in the OEP data trend.

4.3. Generalized gradient approximations

We studied two GGA's with the PBE form. PBEsol has μ matching that of the gradient expansion, while PBE is about double that. The impact seen in Fig. 5 is to improve exchange energies overall, lowering ΔB_{x} and increasing the slope ΔC_{x}. What happens if we should continue the trend? Fig. 6 includes an PBE model that was asymptotic adjusted using the old fit. It has $\mu = 0.2609$, closer to what B88 exchange tends to, and suggested by Ref. 10, but otherwise keeping the same functional form as the PBE and PBEsol. The result (downward triangles) is clearly to overshoot the OEP, with much too steep a slope in the data. Arguably, PBE already had the close to optimal slope in Z for $10 < Z < 120$; attempting to shift the magnitude of the correction to the OEP by changing μ worsens the fit to the data as a function of $\frac{1}{\log Z}$.

Model	μ	ΔB_x	ΔB_x^{fit}	ΔC_x^{fit}	Ratio
PBEsol	0.1235	9.38	9.22	46.0	4.9
PBE	0.209	16.68	16.60	78.5	4.7
acPBE	0.2609	19.83	20.82	90.3	4.5
B88	0.275	20.9		90.8	4.3
Theory		25.33		56.0	2.2

TABLE I. Results of analysis of the large-Z limit of various GGAs described in the text. μ is the coefficient of the gradient expansion used in each functional, ΔB_x, the theoretical value of the logarithmic coefficient derived from the gradient expansion, ΔB_x^{fit} and ΔC_x^{fit} are the results of fitting GGA data to Eq. (9) for PBE and its variants, or to Eq. (eq:delexb88) for B88. Ratio is the ratio $\Delta C_\text{x}^{fit}/\Delta B_\text{x}$. Asymptotic coefficients are reported in mHa.

Secondly, we can verify that the linear extrapolations to $x = 0$ that we made in Fig. 5 (shown again in Fig. 6 as solid lines) hold up, at least for the PBE-like functionals. Clearly, the y-axis intercepts nearly exactly reproduce those predicted from theory for the gradient expansion of each model. This confirms that all these models approach their asymptotic limits fairly quickly. This also gives us confidence that we can make reasonable estimates for the slope (or the ΔC_x coefficient in the asymptotic analysis). The results are summarized in the following table. We see that ΔC_x as well as B in the PBE "family" of GGA's varies roughly linearly with μ, with a nearly constant ratio of $\Delta C_\text{x}/\Delta B_\text{x}$. Interestingly, this ratio is double that predicted by our semi-theoretical model, indicating that no PBE-like functional could capture the basic trend in exchange data well. In this context, PBE is perhaps the best choice since it balances errors in ΔB_x and ΔC_x roughly evenly.

We turn next to B88, which has designed on very different principles, including fitting one parameter to the exchange energies of the noble gas series. Clearly B88 matches OEP very well for $10 < Z < 120$, as is well known. The main issue is a poor description of oscillations, particularly that of the first row atoms needed for organic chemistry. Thus, if we follow the protocol for obtaining ΔB_x and ΔC_x that we used for the OEP, using the same data set of selected closed-shell atoms between $Z = 20$ and 120, we find $\Delta B_\text{x}^{\text{B88}} = 25.72(9)$ mHa, $\Delta C_\text{x}^{\text{B88}} = 55.0(4)$, close to our derived results of Eq. (25). (Interestingly this fit does not extrapolate as well to the B88 data in the first row as it does the OEP data.)

On the other hand, if we follow B88 for $x < 0.2$, i.e., $Z > 120$, we find it soon begins to deviate from this trend. Ultimately the asymptotic trend has to match a y intercept consistent with $\Delta B_\text{x}^{\text{B88}} = 20.9$, the theoretical value derived by expanding the B88 functional about small s^2, and roughly 4 mHa higher than the ΔB_x value predicted by our work. That is to say, the asymptotic trend of beyond-LDA exchange in B88 is to some extent only reached for Z's larger than those we have OEP data for.

To check that this is reasonable, we fit beyond LDA ex-

change for B88 to the form

$$\Delta E_\text{x}^{\text{B88}} = -Z \left(\frac{3}{4\pi^2} \mu^{\text{B88}} \ln Z + \Delta C_\text{x}^{\text{B88}} \right) \\ - Z^{2/3} \left(\Delta D_\text{x}^{\text{B88}} \ln Z + \Delta E_\text{x}^{\text{B88}} \right) \tag{27}$$

finding $\Delta C_\text{x}^{\text{B88}} = 90.8$ mHa, $\Delta D_\text{x}^{\text{B88}} = -4.18$, and $\Delta E_\text{x}^{\text{B88}} = -46.5$ for $Z > 12$. This is shown as a yellow dashed curve and gives a plausible if imperfect fit to the BLYP data for $Z > 12$, failing for small Z. The ΔC_x coefficient is quite plausible, yielding a $4.3 : 1$ ratio for $\Delta C_\text{x}/\Delta B_\text{x}$, close to that of the PBE-like functionals.

This analysis suggests somewhat disquietingly two possible scenarios for OEP exchange. One is our picture – that it is described by a simple and highly accurate asymptotic model one which B88 only matches within the range of data $10 < Z < 100$ for which it was fit. Or, since our own model ultimately relies on its unusual fidelity to OEP data for $1 < Z < 120$, the opposite might be true – the true asymptotic behavior for beyond LDA OEP might not make itself apparent until $Z \gg 100$ and the behavior relevant for real electronic structure might involve a large number of subdominant terms that would be quite hard to determine by any means. B88 or something near it could be the asymptotically correct picture. Ultimately, we will need a fully *a priori* determination of ΔB_x to decide between these two scenarios.

4.4.   meta-GGAs

We finish our discussion of beyond-local results with a short analysis of meta-GGAs. A meta-GGA relies on three semilocal arguments: $n(\mathbf{r})$, $\nabla n(\mathbf{r})$, and $\alpha(\mathbf{r})$. The last of these introduces the noninteracting KE density τ_s:

$$\alpha = \frac{\tau_\text{s} - \tau^{\text{W}}}{\tau^{\text{TF}}} \tag{28}$$

where $\tau_\text{s} = \frac{1}{2} \sum_i^N \nabla \phi(\mathbf{r})^2$ is the positive definite kinetic energy density, and $\tau^{\text{W}} = \frac{1}{2}|\nabla \sqrt{n}|^2$, the von-Weizsäcker kinetic energy density, is its form for a single orbital system. Among recent metaGGAs, TPSS [36] and its derivatives and SCAN[17] are designed to recover the fourth-order gradient expansion for E_x for the slowly varying gas, while others such as r^{2}SCAN[37] and MVS[38] do not. But in all cases, as α modifies only the fourth-order gradient correction, it does not modify ΔB_x.

There is one thing we can take from this. For the bulk of the atom core, α is closely approximated by its gradient expansion [39, 40], and has the form [41, 42]

$$\alpha \sim 1 - \frac{45}{27}s^2 + \frac{20}{9}q. \tag{29}$$

For the inner core, with scaled radius $x = Z^{1/3}r/a < 1$, we also have $q = s^2/3$ so $\alpha \sim 1 - \frac{25}{27}s^2$ and is a redundant parameter. But given the constraint that $\tau_\text{s} > \tau^{\text{W}}$, [43] we

require $\alpha > 0$. This is broken for small x for the value of s^2 equal to $a_1^2/(Z^{2/3}x_1) = 27/25$. and suggests a value for the short-range cutoff parameter x_1 in Eq. 23:

$$x_1 = \frac{25}{27}a_1^2. \tag{30}$$

With this, the leading order correction due to the divergence of n^{TF} and s^2 in the inner core becomes

$$\Delta C_4^{\mathrm{GEA}} \sim \frac{243}{200\pi^2}\mu_4 \tag{31}$$

where

$$\mu_4 = \mu_{pp} + \mu_{pq}/3 + \mu_{qq}/9 \sim 0.06809 \tag{32}$$

using canonical values,[23] resulting in a contribution of about 8 mHA to ΔC_{x}. This is about 20% of the overall ΔC_{x} obtained by numerical analysis of atomic data. This reinforces our finding that the GGA itself dominates the beyond-LDA exchange energies, in that it whows that not only ΔB_{x} is unaffected, but also ΔC_{x} is affected only to a modest extent.

5.   ASYMPTOTICS OF LDA

Surprisingly, the asymptotics of the LDA exchange energies are more difficult to capture than the beyond-LDA corrections. This is because LDA exchange energies have strong oscillations across the periodic table, presumably due to the varying nature of open shells across a row. Because of the KS construction, presumably LDA itself produces extremely accurate densities, with only very insignificant changes (for our purposes) when more sophisticated approximations are used.

5.1.   Basics

Because of the complicated shell structure seen in Fig. 2 it is worthwhile to investigate the asymptotic expansion for the KS LDA. Fig. 7 shows the difference between the LSDA and asymptotic LDA energies per electron, $E_{\mathrm{x}}^{\mathrm{LBA}}/Z$, for all atoms up to $Z = 120$ and for those atoms with closed s, p, d, f, g, h, i, or j valence shells up to $Z = 978$ The data covers 16 rows of the extended periodic table and the $17s^2$ alkali earth. There is a clear (but complicated) oscillatory pattern, superimposed upon a gradual upward drift in energy. The oscillatory pattern has eight peaks indicating the period is every two rows of the periodic table, and the amplitude grows with Z. Note that the changes within one oscillation dwarf those of the beyond LDA term ΔE_{x} discussed in the previous section.

Since we are considering the error in energy for a fixed functional form, Dirac exchange of Eq. 10, any difference from the Thomas-Fermi asymptotic limit is due to density differences. This figure demonstrates the effect caused by introducing shell structure into the density, as compared to
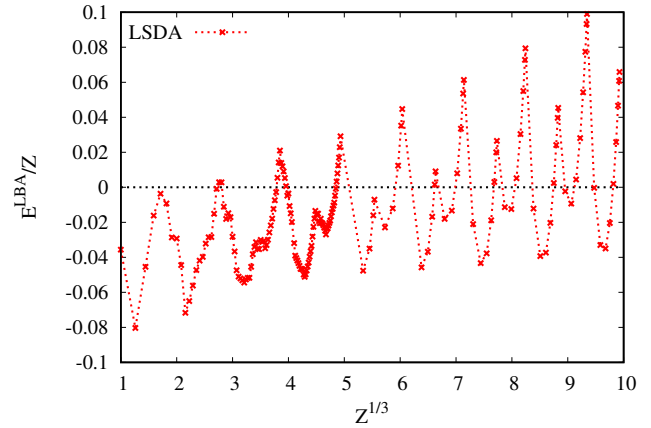
FIG. 7. The LSDA exchange for neutral atoms up to $Z = 120$ and closed-shell neutral atoms up to $Z = 978$, as described in the text, versus $Z^{1/3}$
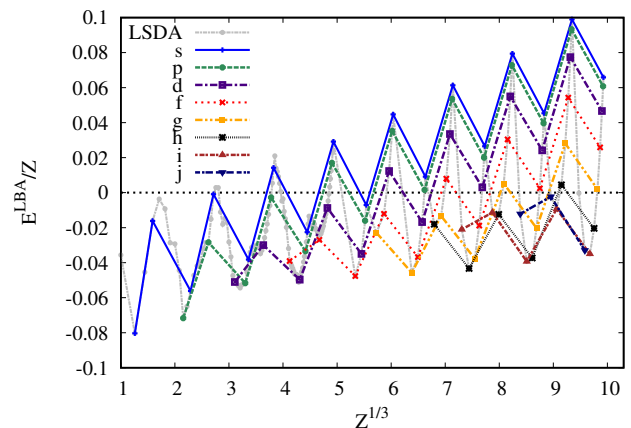
FIG. 8. Plots of the beyond-asymptotic LDA exchange for atoms up to $Z = 120$ and all closed-shell atoms up to $Z = 978$. Overlaid are energies sorted by column of the periodic table. s indicates column 2 with closed s valence shell (alkali earths), p, noble gases, d, group 12 closed d shell atoms, etc. g through j refer to total angular momenta l from 4 to 7, possible in the extended periodic table.

the smooth TF scaling form responsible for the leading order term in exchange.

In Fig. 8 we recast the LDA data to bring out some of the hidden structure underlying the complex oscillatory patterns exhibited by the full data set. We do so by highlighting atoms that belong to columns of the periodic table corresponding to closed-shell systems. These include He plus the alkali earths (with an outermost closed s shell), noble gases (closed p shells), group 12 metals (closed d shells), and continuing up to closed j valence-shell atoms. (The j shell corresponds to total angular momentum $l = 7$ and, according to Madelung's rule, is first occupied in the 15th row of the extended periodic table.) Each column is highlighted by a line joining atoms of that column.

Each column thus displayed forms a stair case pattern that differentiates even and odd rows of the periodic table, falling into a fairly predictable amplitude oscillation after first one or two rows of each column. The g and h closed-shell series of the extended periodic table appear to break this pattern, but because the numerical calculation of the first occurence of these columns (i.e., the 5g and 6h valence shells) failed to converge. The pattern resets each time a new angular momemtum is added to the atomic configuration.

The alkali-earth staircase seems to determine approximately the higher energy edge of the oscillatory pattern of the atomic exchange energy (Fig. 7, and the background in gray in Fig. 8). This is true both for even rows and odd, with the even rows forming the upper limit of the overall pattern. The low-energy edge of Fig. 7 is shown in Fig. 8 to be due to successive low-Z rows of each closed shell column, the first, an atom (He) with s frontier orbitals, then p (Ne), then two with d-shell valence (3d and 4d) and thereafter, a new value of l_{HO} for each minimum. It also seems that each column of closed-shell atoms are slowly converging to the alkali earth case, migrating slowly from the low-energy edge of the exchange energy oscillations to the high-energy.

This last feature can be brought ought more plainly by considering trends versus quantum number rather than $Z^{1/3}$. We first note that closed-shell columns with the same value of the combination $n_{HO} + l_{HO}$, involving the principle quantum number and total angular momentum quantum number of the highest occupied atomic orbital, are located at a fixed distance from each other in the periodic table. Thus, the n_{HO}-s closed-shell atom is two columns from the closed-shell $(n_{HO}-1)$-p atom, which is six columns from $(n_{HO}-2)$d, etc. As n_{HO} and $Z \to \infty$, the length of each row of the periodic table also diverges to infinity, and so these fixed differences become negigibly small fractions of an oscillation in Fig. 7. Thus $n_{HO} + l_{HO}$ yields a proxy for $Z^{1/3}$, one that is easier to construct a model for, and which allows a direct comparison between atoms in different colunns.

As we can directly compare atoms across different columns of the periodic table which have the same value of $n_{HO} + l_{HO}$, it is instructive to plot the exchange energy-per-electron for each closed-shell column in our data set relative to that of the alkali earths, as shown in Fig. 9. This shows clear and reasonably smooth convergence of the p and d series to the alkali earths, while the higher l_{HO} columns seem to swerve away for a few cycles before falling into line. It seems likely that all the columns will share the same asymptotic slope (i.e., leading order trend) in Fig. 8 as the alkali earths, but possibly have somewhat different asymptotes. The oscillatory part of each column seems also to converge onto the alkali earth pattern, more slowly for the higher l_{HO} columns.
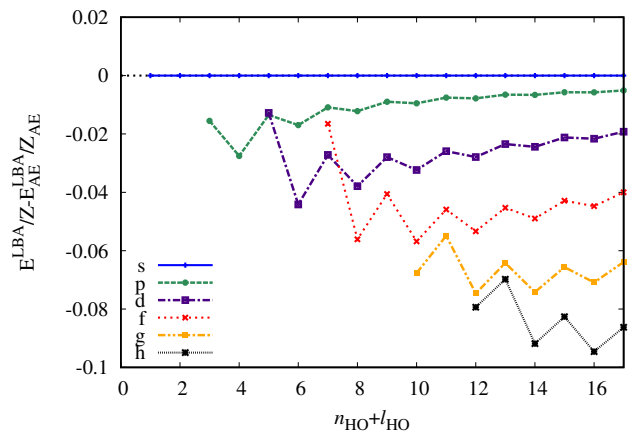
FIG. 9. LDA exchange energy per electron for several closed-shell columns of the extended periodic table, measured relative to that of the nearest alkali earth atom. Difference between LDA exchange energy per atom and that of He and the alkali earth with the same $n_{HO} + l_{HO}$, where n_{HO} is the principle quantum number and l_{HO} is the angular momentum quantum number. p stands for closed p-shell atoms (noble gases), etc.

5.2. Model for the large-Z expansion of the alkali earth series

The previous figures suggest a protocol for extracting the leading order coefficient for the beyond-asymptotic exchange of the LDA. As $Z \to \infty$ or equivalently, $n_{HO} \to \infty$ for any closed-shell column of the periodic table (fixed l_{HO}), we hypothesize the staircase trend should gradually merge with that of the alkali earths and thus the leading order for a given column should be given by that of the alkali earths. It is quite possible that lower-order terms should still be l-dependent. From the visual analysis of the alkali earths, it seems apparent that the leading order term for beyond-TF LDA for this column should be of order $Z^{1/3}$ or equivalently, $n_{HO} + l_{HO}$ – the straight-line behavior not seen in Fig. 3. In addition, as the oscillations between even and odd filled-shell atoms are exactly periodic vs principle quantum number n_{HO}, we can model then with a simple oscillatory term. As there is little evidence that the oscillation amplitude grows with n_{HO} we posit the following extension of the large-Z expansion, written parametrically in terms of highest-occupied shell quantum numbers $n_{HO}(Z)$ and $l_{HO}(Z)$:

$$E_{fit}^{LBA}/Z \to \mathcal{A}\xi + \mathcal{B}\ln(\xi) + \left[\mathcal{C} + \delta\mathcal{C}(-1)^{\xi}\right] \\ + \mathcal{D}/\xi + \mathcal{E}\ln\xi/\xi + \cdots \tag{33}$$

where $\xi = n_{HO} + l_{HO}$, so that $\xi = n_{HO}$ for Helium and the alkali earths. Given the existence of a $\ln Z$ term for beyond-LDA exchange, we have added the possibility of a log term; otherwise the expression is equivalent to an expansion in powers of $Z^{1/3}$. We can also consider higher order terms of order $(n_{HO} + l_{HO})^{-1}$, equivalent to $Z^{-1/3}$.

10
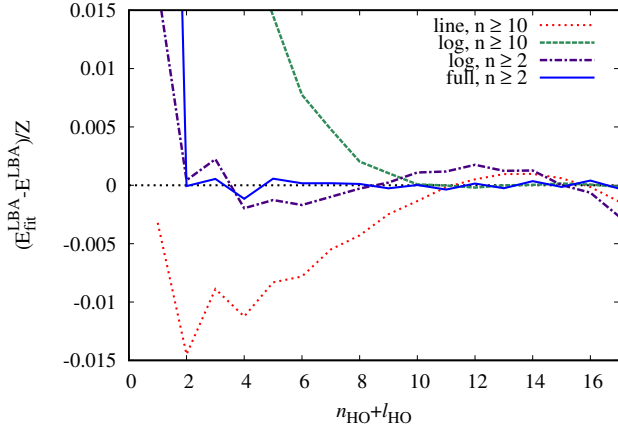
FIG. 10. Difference of the LDA vs n_{HO} for He and alkali earth atoms and various fits of the form Eq. 33, as described in the text and in Table II.

To ascertain the most likely form of the asymptotic expansion of LDA exchange for the alkali earth series, we compare statistical fits to various models with terms down to $O(1)$ in ξ, an exercise similar to that carried out for beyond-local exchange in Ref. 21. We first restrict our fits to values of $n_{\mathrm{HO}} \geq 10$, restricting our focus to higher Z while keeping a reasonable number of data points. This should help maximize the footprint of the leading terms in the LDA asymptotic series, and allow us to truncate higher-order terms.

Since the trend in data for a given column is extremely smooth, the quality of a fit is not easily tested by usual statistical measures, so we judge by visual comparison, as shown in Fig. 10. This shows the deviation of various least-square fits of the LDA exchange energy per electron for the AE series. These include a purely linear trend (labeled "line"), with logarithmic coefficient $\mathcal{B}$ set to zero in Eq. (33), and one with both linear and log trends ("log"). Fit coefficients for these fits are Fits with $\mathcal{A} = 0$ were clearly poorer and are not shown. (More details on statistical fits and a complete list of models we considered are shown in supplemental information.

Note that the error of the purely linear fit has noticeable curvature and thus the reported coefficient $\mathcal{A} = 0.009$ or 9 mHA must be an underestimate of the slope. Adding the logarithmic term greatly improves the fit to the data, basically reproducing the trend within numerical error for $n_{\mathrm{HO}} \geq 10$, and suggesting a value for the leading order coefficient of $\mathcal{A} = 14$ mHa.

Table II shows coefficients of fits for several columns of the periodic table in addition to the alkali earths – corresponding to filled p, d and f valence shells. While the coefficient $\mathcal{A}$ is somewhat sensitive to the form of the asymptotic expansion taken, it is roughly independent of column. Other coefficients are understandably less reliable, except for the amplitude of the even-row to odd-row oscillation. This is quite stable for all columns of the table, all fit ranges and model forms.

Next, as a verification of the robustness of the fit param-

eters we find, we repeat our calculation over a greater range of data, including all points with $n_{\mathrm{HO}} \geq 2$. Fit 6 of Table II ("log, $n \geq 2$" in Fig. 10) is the same functional form as fit 2 in the table, but now it is seen to be unable to capture the observed trend at large Z. To do so, we need to add two additional sub-dominant terms in the series: $\mathcal{D}/\xi + \mathcal{E}\ln\xi/\xi$. These results are shown as fit 7 in Table II and labeled as "full" in Fig. 10, which shows that the resulting error is very nearly reduced to small fluctuations for all rows except $n_{\mathrm{HO}} = 1$. The penalty is that now, the leading order coefficient has changed yet again, to $\mathcal{A} = 20$ mHa.

This result raises an essential problem limiting further progress – the LDA exchange is inherently much more complicated than the beyond-LDA series. In addition to the many terms needed, the presence of both logarithmic and power law terms means that an accurate asymptotic trend will be hard to determine even with the extended range of data we have for the LDA, and overfitting is a clear danger. Thus unfortunately, we do not expect our exercise to yield an unambiguous value for $\mathcal{A}$, and even less for $\mathcal{B}$ or other subleading terms.

Nevertheless, we should like our results for the alkali earths to be expressed as an expansion in n_{HO} converted into a conventional function of Z. The Z value for alkali earths for even rows of the periodic table (valence shell configurations of $2s^2$, $4s^2$, $6s^2$, etc.) is given exactly by

$$Z_{AE}(j) = \sum_{k=1}^{j}(2k)^2 = \frac{2}{3}j(j+1)(2j+1) \qquad (34)$$

where the principle quantum number of the highest-occupied shell is $n_{\mathrm{HO}} = 2j$, and j is an integer. For any of the other series, take $j = (n_{\mathrm{HO}} + l_{\mathrm{HO}})/2 (= \xi/2)$. Then

$$Z_l(j) = Z_{AE}(j) - 2l_{\mathrm{HO}}^2. \qquad (35)$$

We then consider j as a continuous variable and invert $Z_{AE}(j)$ to find, exactly for even-row alkali earths:

$$j(Z_{AE}) + \frac{1}{2} =$$

$$+ \left\{ \left(\frac{3Z_{AE}}{8}\right) + \left[\left(\frac{3Z_{AE}}{8}\right)^2 - \left(\frac{1}{12}\right)^3\right]^{1/2} \right\}^{1/3} \qquad (36)$$

$$+ \left\{ \left(\frac{3Z_{AE}}{8}\right) - \left[\left(\frac{3Z_{AE}}{8}\right)^2 - \left(\frac{1}{12}\right)^3\right]^{1/2} \right\}^{1/3}$$

Now this expression yields an asymptotic expansion for j in Z. In fact, Eq. 34 matches that for the summation of the total kinetic energy of a hydrogenic or Bohr atom (one with noninteracting particles feeling a central Coulomb potential.) From this, one can derive [12] the following expansion:

$$j_{AE}^{even}(Z) = z - \frac{1}{2} + \frac{1}{12z} + ... \qquad (37)$$

where $z = (3Z/4)^{1/3}$. For even-row atoms, E_{fit}^{LBA}/Z then

TABLE II. Table of fit parameters to the beyond-asymptotic contribution to the LDA exchange energy $E_{\mathrm{x}}^{\mathrm{LBA}}$ for closed-shell atoms segregated by valence angular momentum l_{HO}. First column gives the angular momentum for highest occupied orbital Second column gives the minimum value of $\xi = n_{\mathrm{HO}} + l_{\mathrm{HO}}$ used in the fit. Missing coefficients indicate the coefficient has been fixed at zero. Fits are done by Levenberg-Marquardt method, with error in statistical fit given in parentheses.

l_{HO}	n_{HO}	$\mathcal{A}$	$\mathcal{B}$	$\mathcal{C}$	$\delta\mathcal{C}$	$\mathcal{D}$	$\mathcal{E}$
0	≥ 10	0.00925(18)		-0.0709(24)	0.0218(4)		
0	≥ 10	0.01433(31)	-0.068(4)	0.035(6)	0.02180(5)		
1	≥ 10	0.0134(5)	-0.048(7)	-0.010(11)	0.02147(9)		
2	≥ 10	0.0124(15)	-0.021(20)	-0.082(32)	0.02049(27)		
3	≥ 12	0.013(4)	-0.016(6)	-0.12(10)	0.0195(4)		
0	≥ 2	0.00944(32)	-0.0087(24)	-0.0507(23)	0.0221(4)		
0	≥ 2	0.0203(11)	-0.282(30)	0.70(8)	0.02220(14)	-0.68(7)	-0.71(8)

becomes

$$E_{fit}^{LBA}/Z \to 2\mathcal{A}z + \mathcal{B}\ln(2(z - 1/2 + (12z)^{-1}))$$
$$(\mathcal{C} + \delta\mathcal{C} - \mathcal{A}) + 2\mathcal{A}(12z)^{-1} \quad (38)$$

Expanding the log term to order z^{-1} and converting z to Z produces the expression

$$E_{fit}^{LBA}/Z \approx A_{\mathrm{x}}^{\mathrm{LDA}}Z^{1/3} + B_{\mathrm{x}}^{\mathrm{LDA}}\ln(Z) + C_{\mathrm{x}}^{\mathrm{LDA}} + D_{\mathrm{x}}^{\mathrm{LDA}}Z^{-1/3} \quad (39)$$

where $A_{\mathrm{x}}^{\mathrm{LDA}} = 6^{1/3}\mathcal{A}$. For the two best fits to the alkali earths discussed in the text – fit 2 and fit 7 of Table II we end up $A_{\mathrm{x}}^{\mathrm{LDA}} = 25$ and 36 mHa respectively. For odd-row alkali earths, the appropriate asymptotic expansion is that with $\delta\mathcal{C}$ replaced by $-\delta\mathcal{C}$ in Eq. 38. But in addition, one has to alter the asymptotic map from Z to j to

$$j_{AE}^{odd}(Z) = z - \frac{1}{2} - \frac{1}{6z} + ... \quad (40)$$

Inspection shows that if we use this expression to determine the odd rows, the leading order terms in Eq. (39) are unchanged, but terms starting with $D_{\mathrm{x}}^{\mathrm{LDA}}$ will change dramatically. This is a small discrepancy but will complicate the formulation of the column-dependent correction to our fit.

Figure 11 is a reprise of Fig. 7 showing various fits to the even n_{HO} filled s-shell series of the form of Eq. 38. The basic linear fit, fit 1 of Table II, already captures the rough trend of the data; the remaining error is reasonably small. The second fit of table II which includes a logarithmic term (non-zero $\mathcal{B}$), seems to capture the large Z asymptotics particularly well, given both figures 10 and 11, but diverges for small Z. When including lower shell data in fits, complicated transient features become apparent, for example the region in between $2 \geq Z^{1/3} \leq 6$. These are fit well by fit 7 of Table II, ("full, $n \geq 2$" in Fig. 7), with six fitting parameters. These, however, may be the result of higher order oscillatory terms not captured well by the single oscillatory term $\delta\mathcal{C}$. We also note that this fit is not nearly as good as fit 2 for large Z. This suggests that fit 2 gives the best predictions of $\mathcal{A}$ and $\mathcal{B}$ for the large Z asymptotic expansion.
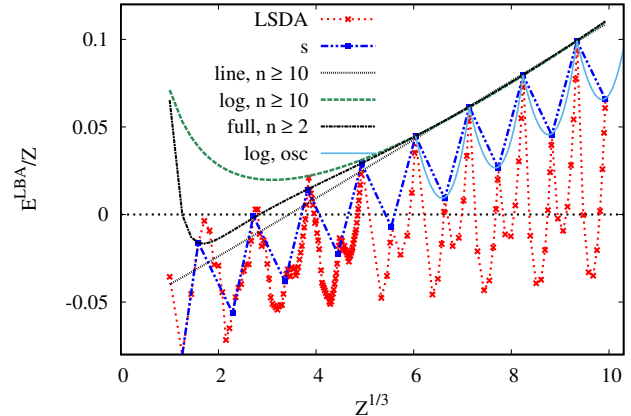
FIG. 11. The beyond asymptotic component of the LSDA (E^{LBA}) plotted vs $Z^{1/3}$ (red) with He and the alkali earths highlighted (blue); along with various fits parametrized in Table II discussed in the text. The LSDA data for filled s-shell atoms is highlighted in blue. Fits shown are fit 1 of Table II ("line, $n \geq 10$"), fit 2 ("log, $n \geq 10$"), and fit 7 ("full, $n \geq 2$"). Light blue shows the oscillatory extension of fit 2 discussed in Sec. 5.3.

5.3. Oscillatory terms

We finish with a short discussion of what issues are involved with characterizing the full oscillatory pattern in the beyond-asymptotic LDA. From Fig. 7 and 8, we have a period that takes up two rows of the periodic table, broken up into an even-row and odd-row sub-pattern. To characterize this pattern, we construct a variable $\nu(Z)$ describing the partial occupation over a two-row period which varies uniformly between zero and one between two even-row alkali earths, taking the value $1/2$ at the odd-row alkali earth. Similarly, one may need a variable $\lambda(Z)$ that does the same on a per-row basis. The function $j_{AE}^{even}(Z)$ that we used to convert our smooth fit in n_{HO} to the alkali earths may be converted to a function of Z usable over the entire periodic table using an asymptotic expansion that depends on both

Z and ν:[1, 12]

$$j(Z,\nu) = z - \frac{1}{2} + \frac{1 - 12\nu(1-\nu)}{12z} \qquad (41)$$

With this formula, we can construct a single model for all the alkali earths, including oscillatory effects, as

$$E^{\text{LBA}}/Z \rightarrow \mathcal{A}2j(Z,\nu) + \mathcal{B}\ln[2j(Z,\nu)] + \mathcal{C} + \delta\mathcal{C}[1 - 8\nu(1-\nu)]. \qquad (42)$$

In the last term, we include an ν-dependence similar to that of Eq. (41). This is shown in Fig. 11 in light blue, using fit 2 of Table II, for rows with n_{HO} greater than 10. The agreement for all alkali earths is quite good.

A full model of the entire periodic table will require a good model for the low-energy edge of the oscillatory pattern. This lower edge has limited data for which our calculations prove to be less numerically reliable. Preliminary work suggests that this could be fit by a logarithmic term shifted by a constant – that is, with no $Z^{1/3}$ term.

6. DISCUSSION

This paper follows up on a report [21] and analysis of the conjectured $Z\ln Z$ term in the large-Z asymptotic expansion of the beyond-LDA contribution to exchange energies of neutral atoms. A simple model for this contribution on a per-electron basis is thus $\Delta E_{\text{x}}/Z \sim \Delta B_{\text{x}}\ln Z + \Delta C_{\text{x}}$ where ΔB_{x} is taken to be 3/4 that derived from the Bohr atom and ΔC_{x} is the beyond-LDA exchange energy of the hydrogen atom. This paper analyzes to what extent these beyond-LDA results are amenable to analysis by popular forms of density functional theory such as GGAs and meta-GGAs and also describes the LDA exchange energies themselves, particularly determining a $Z^{4/3}$ behavior for the leading correction to the local limit. These studies demonstrate significant complications beyond what can be predicted by tools such as dimensional analysis and models such as the gradient expansion.

Some perspective on these results may be obtained by reconsidering the Lieb-Simon scaling that we began our story with. This process is a scaling of the potential, but there also exists dual procedure of density scaling:

$$n_\zeta(\mathbf{r}) = \zeta^2 n(\zeta^{1/3}\mathbf{r}). \qquad (43)$$

which differs from the usual coordinate scaling in DFT, as the number of particles changes. Within TF theory, the scaled density is the ground-state of the scaled potential, but this is not true more generally.

Early work analyzing the asymptotic form of exchange[10, 19] took the approach of density scaling, and the exact density weakly approaches the TF density in the limit of large Z. (Weakly here means sufficiently smooth integrals over the exact density approach zero relative error when evaluated with the TF density.) Moreover, the relative error in the TF total energy also vanishes. Assuming (incorrectly) that differences between the exact and approximate densities would

contribute mainly to higher orders and to oscillations in the exchange energy characteristic of the LDA, suggests

$$E_{\text{x}} \rightarrow -d_0 Z^{5/3} - \Delta C_{\text{x}} Z + \cdots \qquad (44)$$

for exchange. In fact, the beyond-LDA data was tested to include a $Z^{4/3}$ term, but its coefficient was found to be numerically indistinguishable from zero[10].

The LS theorem guarantees weak convergence to the TF limit for the total energy and the results of Schwinger[8] and Conlon[9] imply a similar principle for the leading contribution to the exchange energy. However, beyond such dominant terms, whether or not the gradient expansion can yield the next subdominant correction is a delicate question. The gradient expansion for the (non-interacting) kinetic energy *does* yield the exact contribution to the $Z^{5/3}$ in the total energy, without modification. Table I shows that the true gradient expansion limit, implemented by PBEsol gets ΔC_{x} closer than any other density functional, (off by 20% at most). Our estimate for the fourth-order gradient expansion contribution to this quantity, about 8 mHa, almost exactly makes up this deficit. What the gradient expansion does not predict properly, either for kinetic energy or for exchange is an additional anomalous term not predictable from density scaling – the Scott term of order Z^2 for the former and the $Z\ln Z$ term for exchange.

A contrast could be made to the situation with quantum dots[11], whose asymptotic series for the total energy and for exchange each have the same form as that generated by density scaling. It remains an open question what should be the necessary conditions in a scaled potential for anomalous powers to appear in the associated asymptotic series.

6.1. Semilocal approximations

The analysis of semilocal density functionals adds nuance to our prior conclusions. First, the logarithmic term for the exchange energy-per-particle in such a model is uniquely determined by its second-order gradient expansion in the limit of a slowly varying density, and the coefficient, ΔB_{x}, by the coefficient μ of this correction. But also the second coefficient ΔC_{x} is roughly linear in μ as well. A GGA thus has the task of attempting to fit two asymptotic coefficients with one adjustable parameter. This task is made more difficult in that the value of μ, $1/3$, needed to obtain the B coefficient of our model, is significantly larger than any encountered in a successful GGA. What a successful GGA like PBE or BLYP does is find a useful compromise between obtaining an accurate value for ΔB_{x} and one for ΔC_{x} by choosing a μ somewhere between the correct value and that needed to match asympototics of the large-Z atom. In contrast, as discussed above, the implementation of the exact gradient expansion limit matches ΔC_{x} reasonably while introducing large errors in ΔB_{x}.

In contrast, metaGGAs have the flexibility to match both ΔB_{x} and ΔC_{x} because they incorporate explicit control over the second-order and fourth-order gradient expansion

corrections to the LDA. But doing so likely produces coefficients quite far from those optimal for a slowly-varying periodic system. It is uncertain whether this would be a profitable thing to do.

But all these conclusions are limited by the limited range of our data and capacity of our theoretical methods to determine the exact asymptotic behavior of atoms. We have seen that one could generate an alternate model supposing B88 exchange to be the correct picture, with behavior for $Z < 100$ determined by a large number of subdominant terms in an asymptotic expansion while the leading terms only becoming dominant for $Z \gg 100$. The need for such subdominant terms to describe B88's asymptotic behavior is likely due to its complicated form as a function of s^2. We cannot prove that they are not there for exact exchange. Rather, our conclusions stand on the surprising accuracy of our simple two parameter fit, consistent with the expectation that asymptotic expansions are efficient.

6.2. Outcomes for LDA

A full picture of the asymptotic expansion of exchange involves the description of LDA exchange beyond the TF approximation. The result is a rich and complex oscillatory pattern showing the full complexity of the periodic table and which we only start to unravel.

Because of the need to consider logarithmic terms in our modeling, we are unable to get a definitive fit, even for a smooth average trend, in the fashion of the beyond-LDA data. This awaits accurate accurate exchange data at much larger values of Z. But we are able to make a number of conclusions – primarily that the leading beyond-TF term in exchange of neutral atoms is of order $Z^{4/3}$. The value of the coefficient depends on the fit strategy used but is likely between 10 to 20 mHa. This estimate is made by fitting the data for the alkali earth column and noting that the energy series of any other closed-shell column approaches that of the alkali earths at least to this order.

The overall trend of oscillations is quite complex. The pattern (involving closed-shell atoms only) depends on the fraction of filling of each row of the periodic table superimposed on a trend that takes two rows to repeat. At least for closed-shell systems, the local maxima of this two-row pattern seem to be the even-row and odd-row alkali earths. For this and likely any column of the periodic table there is a distinct oscillation between even and odd rows of the periodic table with an asymptotic form of $\pm\delta\mathcal{C}Z$, for $\delta\mathcal{C} = 22$mHa. The lower boundary is formed by a series of atoms with near minimum $n_{\mathrm{HO}} - l_{\mathrm{HO}}$ – those that nearly maximize the

angular momentum of the valence shell for a given value of $n_{\mathrm{HO}} + l_{\mathrm{HO}}$. The amplitude of the complete oscillatory pattern apparently grows roughly as $Z^{4/3}$, similar to that seen by Englert for the total energy.

The cause of these effects is the appearance of shell structure changing the charge density from the scale-invariant Thomas-Fermi density. The very strong dependence of exchange on the angular momentum quantum number of the frontier shell, as well as common sense consideration of energetics, indicates that these changes should primarily involve the outer shells of the atom. The most notable density change is at large radial distqnces r from the nucleus: from the asymptotic of $1/r^6$ for TF to an exponential decay at finite radius. However, there can be a non-negligible contribution from a large number of outer shells of the atom, as has been seen in a somewhat different context in Ref. [40].

One argument why alkali earths should present the "roof" for exchange energy comes from considering the exchange contribution of the outermost shell. The exchange energy can be expressed as the expectation of the interaction of an electron with its exchange hole – the change in overall electron density elsewhere given the particle is observed at some particular point in space. If this electron is in a valence s-shell, its exchange hole will be diffused over the entire valence region, leading to a relatively weak exchange energy. This could very well be positive relative to that predicted by Thomas-Fermi-Dirac theory. For a frontier shell with a large degree of degeneracy, greater localization of the exchange hole is possible and thus a lower exchange energy.

Although they may not impact development of KS DFT, these issues in the LDA and beyond-LDA energy for exchange illustrate the difficulty of achieving accurate orbital-free models of the energy and its XC component, and point to the large amount of work that still remains to understand the large-Z limit of atoms.

SUPPLEMENTARY MATERIAL

See supplementary material for tables of LSDA and GGA exchange energies, numerical stress tests, additional fit data and additional plots of exchange energies. For OEP data, see the supplementary material of Ref. 21. Additional data is available on request.

ACKNOWLEDGMENTS

[1] B.-G. Englert, Lec. Notes Phys. **300** (1988). 1, 3, 5, 7, 13

[2] L. H. Thomas, Math. Proc. Camb. Phil. Soc. **23**, 542 (1927), URL http://dx.doi.org/10.1017/

S0305004100011683. 1

[3] E. Fermi, Zeitschrift für Physik A Hadrons and Nuclei **48**, 73 (1928), ISSN 0939-7922, URL http://dx.doi.org/10.

1007/BF01351576. 1

[4] D. Lee, L. A. Constantin, J. P. Perdew, and K. Burke, J. Chem. Phys. **130**, 034107 (pages 9) (2009), URL http://link.aip.org/link/?JCP/130/034107/1. 1, 4, 5

[5] E. Lieb and B. Simon, Phys. Rev. Lett. **31**, 681 (1973). 1, 2

[6] E. H. Lieb and B. Simon, Advances in Mathematics **23**, 22 (1977). 1, 2

[7] W. Kohn and L. J. Sham, Phys. Rev. **140**, A1133 (1965), URL http://link.aps.org/doi/10.1103/PhysRev.140.A1133. 1

[8] J. Schwinger, Phys. Rev. A **24**, 2353 (1981). 1, 2, 13

[9] J. Conlon, Communications in Mathematical Physics **88**, 133 (1983), ISSN 0010-3616, URL http://dx.doi.org/10.1007/BF01206884. 2, 13

[10] P. Elliott and K. Burke, Can. J. Chem. Ecol. **87**, 1485 (2009), URL http://dx.doi.org/10.1139/V09-095. 1, 2, 3, 7, 13

[11] H. Kunz and R. Rueedi, Phys. Rev. A **81**, 032122 (2010), URL http://link.aps.org/doi/10.1103/PhysRevA.81.032122. 1, 2, 13

[12] K. Burke, A. Cancio, T. Gould, and S. Pittalis, The Journal of Chemical Physics **145**, 054112 (2016), URL http://scitation.aip.org/content/aip/journal/jcp/145/5/10.1063/1.4959126. 3, 5, 11, 13

[13] A. Cancio, G. P. Chen, B. T. Krull, and K. Burke, The Journal of Chemical Physics **149**, 084116 (2018), URL https://aip.scitation.org/doi/10.1063/1.5021597. 1

[14] S. Crisostomo, R. Pederson, J. Kozlowski, B. Khalita, A. Cancio, K. Datchev, A. Wasserman, S. Song, and K. Burke, Letters in Mathematical Physics **113**, 42 (2023), URL https://doi.org/10.1007/s11005-023-01665-z. 1

[15] P. A. M. Dirac, Mathematical Proceedings of the Cambridge Philosophical Society **26**, 376 (1930), URL http://dx.doi.org/10.1017/S0305004100016108. 1

[16] J. P. Perdew, A. Ruzsinszky, G. I. Csonka, O. A. Vydrov, G. E. Scuseria, L. A. Constantin, X. Zhou, and K. Burke, Phys. Rev. Lett. **100**, 136406 (2008), URL http://link.aps.org/doi/10.1103/PhysRevLett.100.136406. 1, 3, 5

[17] J. Sun, A. Ruzsinszky, and J. P. Perdew, Phys. Rev. Lett. **115**, 036402 (2015), URL http://link.aps.org/doi/10.1103/PhysRevLett.115.036402. 1, 8

[18] B.-G. Englert and J. Schwinger, Phys. Rev. A **32**, 47 (1985). 1, 3

[19] J. P. Perdew, L. A. Constantin, E. Sagvolden, and K. Burke, Phys. Rev. Lett. **97**, 223002 (2006), URL https://link.aps.org/doi/10.1103/PhysRevLett.97.223002. 2, 5, 13

[20] T. J. Daas, D. P. Kooi, A. J. A. F. Grooteman, M. Seidl, and P. Gori-Giorgi, Journal of Chemical Theory and Computation **18**, 1584 (2022), https://doi.org/10.1021/acs.jctc.1c01206, URL https://doi.org/10.1021/acs.jctc.1c01206. 2, 3

[21] N. Argaman, J. Redd, A. C. Cancio, and K. Burke, Phys. Rev. Lett. **129**, 153001 (2022), URL https://link.aps.org/doi/10.1103/PhysRevLett.129.153001. 2, 3, 4, 5, 6, 7, 11, 13, 14

[22] K. J. Daas, D. P. Kooi, T. Benyahia, M. Seidl, and P. Gori-Giorgi, *Large-z atoms in the strong-interaction limit of dft: Implications for gradient expansions and for the lieb-oxford bound* (2023), 2211.07512. 2

[23] P. Svendsen and U. von Barth, Phys. Rev. B **54**, 17402 (1996). 2, 4, 9

[24] O. J. Heilmann and E. H. Lieb, Phys. Rev. A **52**, 3628 (1995), URL http://link.aps.org/doi/10.1103/PhysRevA.52.3628. 2

[25] P. Elliott, D. Lee, A. Cangi, and K. Burke, Phys. Rev. Lett. **100**, 256406 (2008). 2

[26] B.-G. Englert and J. Schwinger, Phys. Rev. A **26**, 2322 (1982). 2

[27] B.-G. Englert and J. Schwinger, Phys. Rev. A **32**, 26 (1985). 2

[28] C. Fefferman and L. Seco, Advances in Mathematics **107**, 1 (1994), ISSN 0001-8708, URL http://www.sciencedirect.com/science/article/pii/S0001870884710607. 2

[29] J. P. Perdew, K. Burke, and M. Ernzerhof, Phys. Rev. Lett. **77**, 3865 (1996), *ibid.* **78**, 1396(E) (1997), URL http://dx.doi.org/10.1103/PhysRevLett.77.3865. 3, 5

[30] A. D. Becke, Phys. Rev. A **38**, 3098 (1988), URL http://dx.doi.org/10.1103/PhysRevA.38.3098. 3, 5

[31] R. M. Dreizler and E. K. U. Gross, *Density Functional Theory: An Approach to the Quantum Many-Body Problem* (Springer–Verlag, Berlin, 1990), ISBN 0387519939. 4

[32] P. Okun and K. Burke, *Semiclassics: The hidden theory behind the success of DFT* (World Scientific, 2023), URL https://www.worldscientific.com/doi/abs/10.1142/13303. 5

[33] J. Scott, Philos. Mag. **43**, 859 (1952). 5

[34] E. Engel and R. M. Dreizler, Journal of Computational Chemistry **20**, 31 (1999), ISSN 1096-987X, URL http://dx.doi.org/10.1002/(SICI)1096-987X(19990115)20:1<31::AID-JCC6>3.0.CO;2-P. 6, 16

[35] M. Fuchs and M. Scheffler, Computer Physics Communications **119**, 67 (1999). 6, 16

[36] J. Tao, J. P. Perdew, V. N. Staroverov, and G. E. Scuseria, Phys. Rev. Lett. **91**, 146401 (2003), URL http://link.aps.org/doi/10.1103/PhysRevLett.91.146401. 8

[37] J. W. Furness, A. D. Kaplan, J. Ning, J. P. Perdew, and J. Sun, The Journal of Physical Chemistry Letters **11**, 9248 (2020), pMID: 33073997, https://doi.org/10.1021/acs.jpclett.0c03077, URL https://doi.org/10.1021/acs.jpclett.0c03077. 8

[38] J. Sun, J. P. Perdew, and A. Ruzsinszky, Proceedings of the National Academy of Sciences **112**, 685 (2015), https://www.pnas.org/doi/pdf/10.1073/pnas.1423145112, URL https://www.pnas.org/doi/abs/10.1073/pnas.1423145112. 8

[39] A. C. Cancio and J. J. Redd, Molecular Physics **115**, 618 (2017), https://doi.org/10.1080/00268976.2016.1246757, URL https://doi.org/10.1080/00268976.2016.1246757. 8

[40] J. J. Redd and A. C. Cancio, The Journal of Chemical Physics **155**, 134112 (2021), ISSN 0021-9606, https://pubs.aip.org/aip/jcp/article-pdf/doi/10.1063/5.0059283/16044182/134112_1_online.pdf, URL https://doi.org/10.1063/5.0059283. 8, 14

[41] D. Kirzhnits, Sov. Phys. JETP **5**, 64 (1957). 8

[42] C. H. Hodges, Canadian J. Phys **51**, 1428 (1973). 8

[43] M. Levy and H. Ou-Yang, Phys. Rev. A **38**, 625 (1988). 8

Appendix A: Large Z stress test

As a check on the validity of large Z atomic structure calculations, we have compared the energetics from two independent atomic density functional codes, FHI98PP [35] and OPMKS [34]. The former is done using the default integration grid with geometric growth factor $\gamma = 0.0247$, and and a finer grid $\gamma = 0.123$ as described in the text. Table III shows calculations for the energy eigenvalue of the highest-occupied atomic orbital (HO) of helium and noble gas atoms up to $Z = 976$. These prove to be an energy measure sensitive to numerical issues such as failure to converge to a solution in FHI98PP. PW91 exchange and correlation was used for these calculations.

TABLE III. Comparison of the HO eigenvalue calculated on a coarse and fine grid using FHI98PP and using OPMKS

Z	HO fine grid	HO coarse	OPMKS
2	-0.57025586	-0.57025588	-0.57025583
10	-0.49784696	-0.49784690	-0.49784691
18	-0.38222044	-0.38222035	-0.38222041
36	-0.34625570	-0.34625554	-0.34625569
54	-0.30977911	-0.30977894	-0.30977910
86	-0.29313618	-0.29313608	-0.29313616
118	-0.27392048	-0.27392058	-0.27392045
168	-0.26363740	-0.26363782	-0.26363735
218	-0.25147948	-0.25148038	-0.25147939
290	-0.24426230	-0.24426386	-0.24426218
362	-0.23575844	-0.23576087	-0.23575826
460	-0.23032261	-0.23032611	
558	-0.22397950	-0.22398436	-0.22397916
686	-0.21969293	-0.21969939	
814	-0.21474382	-0.21475225	
976	-0.21125111	-0.21126178	

Appendix B: Energy Data

Tables IV,V,VI,VII give total exchange energies for LSDA exchange calculated by OPMKS for atoms $Z \leq 120$ as well as the LDA for closed shell atoms $Z > 120$ (same as LSDA) for and various GGAs calculated by FHI98PP. GGAs are not spin polarized calculations. An entry of "nan" indicates that the calculation did not converge.

Appendix C: Additional plots

Fig. 12 plots exchange-energy per charge split into columns of the periodic table, plotted vs the principle quantum number of the HO (n_{HO}) plus the angular momentum of the HO (l_{HO}).
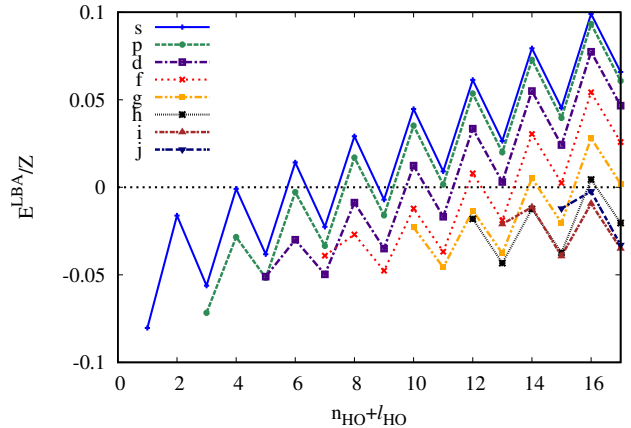
FIG. 12. Plots the difference between KS LSDA exchange energies and TF LDA exchange vs principle quantum number plus the angular momentum quantum number of the last filled shell.

Appendix D: Statistical fits of beyond-asymptotic LDA data

In Table VIII and IX we present statistical fits of a number of models for the beyond-asymptotic component of LDA exchange, defined by Eq. 6 in the main text. The fits are to an expansion in n_{HO}, the principal quantum number of the highest-energy occupied orbital, given by Eq. 33 of the main text, reprised, . Shown in the SI are a number of fits using Levenberg-Marquardt nonlinear regression. If a coefficient is missing, then it has been constrained to be zero. Standard errors are shown in parentheses, along with the χ^2_{red} measure, which is the χ^2 measure of the fit divided by the number of independent data points in the fit. A χ^2_{red} less than $1e-7$ was needed to reduce the error to numerical error rather than systematic error from a wrong fitting function.

TABLE IV. Exchange energies as calculated by FHI98PP in non-relativistic mode using the exchange functional stated, with the exception of the LSDA which was calculated by OPMKS for atoms up to 120, and FHI98PP for higher Z atoms.

Z	PBEsol	PBE	BLYP	LSDA
1	-0.285103	-0.301759	-0.305921	-0.256426
2	-0.952651	-1.005099	-1.018337	-0.861740
3	-1.665161	-1.751734	-1.771358	-1.514295
4	-2.507204	-2.633584	-2.657785	-2.290333
5	-3.527610	-3.695906	-3.726510	-3.246785
6	-4.776838	-4.988579	-5.027871	-4.430191
7	-6.272321	-6.529170	-6.578122	-5.857031
8	-7.790568	-8.100493	-8.154102	-7.300277
9	-9.564857	-9.928070	-9.989481	-8.999038
10	-11.610176	-12.027537	-12.099347	-10.966746
11	-13.451905	-13.924267	-14.006053	-12.729476
12	-15.366169	-15.896179	-15.986368	-14.563428
13	-17.368448	-17.953607	-18.053264	-16.485917
14	-19.507646	-20.148558	-20.259722	-18.544496
15	-21.788564	-22.486058	-22.609315	-20.743147
16	-24.076698	-24.832382	-24.966611	-22.949589
17	-26.515780	-27.330118	-27.475697	-25.305450
18	-29.107513	-29.981392	-30.139415	-27.812161
19	-31.540945	-32.475933	-32.646217	-30.162201
20	-34.021221	-35.018503	-35.200554	-32.559071
21	-36.780064	-37.837632	-38.033415	-35.236844
22	-39.706642	-40.824452	-41.034752	-38.080882
23	nan	nan	-44.438807	-41.332351
24	-46.317208	-47.549392	-47.796449	-44.530068
25	-49.449931	-50.749570	-51.005773	-47.571047
26	-52.794474	-54.158130	-54.429019	-50.832824
27	-56.468921	-57.893017	-58.177009	-54.423184
28	-60.172474	-61.659715	-61.959412	-58.040636
29	-64.040916	-65.591487	-65.907619	-61.822122
30	-67.795918	-69.413739	-69.750274	-65.492277
31	-71.561204	-73.242822	-73.596713	-69.168712
32	-75.407020	-77.151814	-77.524221	-72.925515
33	-79.340876	-81.149203	-81.539986	-76.769192
34	-83.245939	-85.119973	-85.529139	-80.587205
35	-87.256845	-89.195559	-89.622997	-84.509595
36	-91.373178	-93.376894	-93.822814	-88.535671
37	-95.330802	-97.402192	-97.866120	-92.403904
38	-99.315762	-101.455560	-101.937255	-96.299795
39	-103.476697	-105.682558	-106.182519	-100.371730
40	-107.763775	-110.036018	-110.554242	-104.567434
41	-112.378509	-114.712770	-115.251191	-109.089494
42	-116.931623	nan	-119.890641	-113.548978
43	-121.317441	-123.792217	-124.365738	-117.839362
44	-126.040253	-128.580983	-129.170095	-122.470059
45	-130.769236	-133.378702	-133.985919	-127.105429
46	-135.773758	-138.450985	-139.073656	-132.012189
47	-140.574957	-143.322635	-143.967816	-136.721135
48	-145.380020	-148.199147	-148.867528	-141.436736
49	-150.190853	-153.078451	-153.768105	-146.155034
50	-155.069722	-158.024503	-158.736018	-150.941087

TABLE V. Continuation of table IV

Z	PBEsol	PBE	BLYP	LSDA
51	-160.018061	-163.040081	-163.772972	-155.795528
52	-164.934009	-168.025544	-168.779985	-160.621632
53	-169.931908	-173.091264	-173.867222	-165.528358
54	-175.009592	-178.236785	-179.034156	-170.513218
55	-179.942326	-183.240451	-184.058395	-175.353399
56	-184.894972	-188.264447	-189.103066	-180.213928
57	-190.004274	-193.443095	-194.302285	-185.230322
58	-195.966874	-199.472708	-200.354797	-191.103880
59	-201.704369	-205.278758	-206.182989	-196.749306
60	-207.567828	-211.210992	-212.137415	-202.520151
61	-213.555438	-217.267608	-218.216238	-208.414629
62	-219.666426	-223.447845	-224.418680	-214.431982
63	-225.900563	-229.751481	-230.744510	-220.571984
64	-231.775153	-235.696001	-236.712778	-226.355247
65	-238.252463	-242.241569	-243.281721	-232.742716
66	-244.609510	-248.667943	-249.731623	-239.008105
67	-251.088082	-255.216058	-256.303258	-245.394357
68	nan	nan	nan	nan
69	-264.412667	-268.680483	-269.814727	-258.532392
70	-271.260166	-275.598322	-276.756100	-265.285690
71	-277.771794	-282.181033	-283.364169	-271.704359
72	-284.348360	-288.828294	-290.035553	-278.185500
73	-290.992645	-295.543525	-296.774193	-284.732719
74	-297.708352	-302.330639	-303.584266	-291.350064
75	-304.498753	-309.192979	-310.469278	-298.040989
76	-311.211928	-315.978919	-317.279032	-304.661333
77	-318.009788	-322.848525	-324.172348	-311.364319
78	-325.080531	-329.988547	-331.331978	-318.334025
79	-332.076152	-337.056848	-338.423389	-325.230195
80	-338.913998	-343.969612	-345.363313	-331.974258
81	-345.739757	-350.867933	-352.286930	-338.703239
82	-352.617522	-357.816687	-359.261580	-345.483911
83	-359.547982	-364.818090	-366.288284	-352.316191
84	-366.436336	-371.779877	-373.275519	-359.110651
85	-373.389574	-378.804549	-380.325715	-365.968805
86	-380.405332	-385.891604	-387.438058	-372.887890
87	-387.276708	-392.837681	-394.408340	-379.662436
88	-394.159238	-399.795193	-401.390311	-386.448625
89	-401.172455	-406.881313	-408.500740	-393.364763
90	-408.257414	-414.039285	-415.682685	-400.350505
91	-415.962771	-421.816489	-423.485682	-407.960738
92	-423.511974	-429.438950	-431.132767	-415.411065
93	-431.160424	-437.161234	-438.879571	-422.959664
94	-439.263323	-445.339853	-447.080632	-430.955907
95	-447.131841	-453.283617	-455.048726	-438.722078
96	-454.691592	-460.917180	-462.708893	-446.186310
97	-462.776870	-469.075474	-470.892098	-454.172626
98	-470.744149	-477.116833	-478.958906	-462.040969
99	-478.807734	-485.254994	-487.122420	-470.004641
100	-486.967635	-493.489973	-495.382716	-478.063747

TABLE VI. Continuation of table IV

Z	PBEsol	PBE	BLYP	LSDA
101	-495.223960	-501.821863	-503.739936	-486.218473
102	-503.576887	-510.250829	-512.194273	-494.469059
103	-511.446178	-518.196149	-520.164373	-502.235361
104	-519.635752	-526.458925	-528.456391	-510.331367
105	-527.758822	-534.656210	-536.679833	-518.353806
106	-535.943574	-542.915471	-544.964778	-526.436787
107	-544.190875	-551.237690	-553.312318	-534.581323
108	-552.363052	-559.485586	-561.586814	-542.657967
109	-560.605775	-567.802772	-569.930538	-550.803254
110	-568.917955	-576.189296	-578.343265	-559.016307
111	-577.299204	-584.645196	-586.825075	-567.296985
112	-585.749514	-593.170631	-595.376208	-575.645463
113	-593.980585	-601.476876	-603.710328	-583.777322
114	-602.257346	-609.827158	-612.088912	-591.954413
115	-610.579172	-618.222415	-620.511799	-600.175466
116	-618.858735	-626.577875	-628.895045	-608.358631
117	-627.193577	-634.986538	-637.331588	-616.595915
118	-635.580919	-643.447490	-645.820102	-624.884164
119	-643.831869	-651.775518	-654.174451	-633.035711
120	-652.090902	-660.111784	-662.537449	-641.195821
152	nan	nan	nan	-963.24472
162	-1083.90933	-1095.11339	-1098.72977	-1068.78028
168	-1147.97249	-1159.63834	-1163.43702	-1132.23151
170	-1169.18675	-1181.01236	-1184.86899	-1153.24075
188	-1384.59708	-1397.84818	-1402.22911	-1366.74978
202	-1557.45197	-1571.80514	-1576.61687	-1538.13741
212	-1682.21957	-1697.36592	-1702.48740	-1661.85723
218	-1757.04245	-1772.66219	-1777.97727	-1736.05551
220	-1781.83402	-1797.61724	-1802.99384	-1760.63772
260	-2376.19435	-2395.16288	-2401.80899	-2350.77803
274	-2589.51881	-2609.61454	-2616.71921	-2562.60478
284	-2742.42429	-2763.33352	-2770.76685	-2714.43811
290	-2833.92454	-2855.32006	-2862.95786	-2805.29803
292	-2864.25370	-2885.81704	-2893.51987	-2835.41239
314	-3240.26344	-3263.65782	-3272.07848	-3208.99340
332	-3552.85191	-3577.73436	-3586.75994	-3519.60902
346	-3797.70737	-3823.74208	-3833.25001	-3762.93835
356	-3972.78324	-3999.64774	-4009.50028	-3936.92316
362	-4077.50032	-4104.86074	-4114.92699	-4040.98896
364	-4112.23126	-4139.76261	-4149.89687	-4075.50139
390	nan	nan	nan	-4605.39831
412	-5097.33491	-5128.86128	-5140.65967	-5055.32866
430	-5469.85244	-5502.89115	-5515.32025	-5425.84307
444	-5760.25369	-5794.46673	-5807.39807	-5714.69083
454	-5967.44325	-6002.50313	-6015.79310	-5920.76822
460	-6091.30751	-6126.87403	-6140.38596	-6043.96787
462	-6132.40804	-6168.14908	-6181.73168	-6084.84529
488	-6735.70871	-6773.70159	-6788.20765	-6685.16919
510	-7248.40529	-7288.29035	-7303.59062	-7195.36575
528	-7669.19259	-7710.61874	-7726.57631	-7614.11588

TABLE VII. Continuation of table IV

Z	PBEsol	PBE	BLYP	LSDA
542	-7996.59712	-8039.21793	-8055.69704	-7939.94341
552	-8230.01525	-8273.49669	-8290.34771	-8172.23292
558	-8369.56749	-8413.56379	-8430.64452	-8311.11092
560	-8415.89591	-8460.06941	-8477.22332	-8357.21298
590	-9234.38168	-9281.12695	-9299.39917	-9172.31421
616	-9937.37621	-9986.38409	-10005.61560	-9872.32126
638	-10532.65533	-10583.57795	-10603.62717	-10465.07172
656	-11019.81029	-11072.29698	-11093.02306	-10950.16042
670	-11398.21910	-11451.92007	-11473.18306	-11326.96761
680	-11667.81044	-11722.38685	-11744.03273	-11595.41165
686	-11828.98898	-11884.08946	-11905.97160	-11755.90438
688	-11882.51809	-11937.79884	-11959.75631	-11809.20317
718	-12791.86384	-12849.83042	-12872.92584	-12715.00661
744	-13576.69738	-13636.97556	-13661.06586	-13496.79268
766	-14240.29550	-14302.52054	-14327.45705	-14157.82352
784	-14782.68823	-14846.50057	-14872.13589	-14698.12228
798	-15203.72967	-15268.77376	-15294.96212	-15117.54153
808	-15503.64709	-15569.57865	-15596.16114	-15416.29696
814	-15682.99103	-15749.45385	-15776.27923	-15594.94651
816	-15742.57501	-15809.22045	-15836.12330	-15654.29729
850	-16935.40359	-17005.05550	-17033.29559	-16843.17349
880	-17970.11068	-18042.45548	-18071.86437	-17874.33172
906	-18863.19591	-18937.87275	-18968.29738	-18764.34310
928	-19617.28734	-19693.93415	-19725.22376	-19515.83775
946	-20232.98309	-20311.23839	-20343.24266	-20129.41253
960	-20710.64290	-20790.14767	-20822.71743	-20605.42779
970	-21050.83029	-21131.23561	-21164.20853	-20944.43646
976	-21254.28367	-21335.22837	-21368.44955	-21147.18516
978	-21321.89884	-21403.02885	-21436.32926	-21214.56365

$\mathcal{A}$	$\mathcal{B}$	$\mathcal{C}$	$\delta\mathcal{C}$	$\mathcal{D}$	$\mathcal{E}$	$\chi^2_{red} \times 10^{-6}$
0.00925(18)		-0.0710(24)	0.02183(4)			1.2
	0.122(7)	-0.261(17)	0.0218(11)			9.9
0.01433(31)	-0.067(4)	0.035(6)	0.02180(5)			0.023
0.01176(21)		-0.138(6)	0.02179(7)	0.434(36)		0.042
	0.309(12)	-0.93(4)	0.02172(16)	2.42(16)		0.21
0.0209(14)	-0.242(36)	0.48(9)	0.021844(23)	-1.13(23)		0.003
0.050(12)	-1.8(6)	6.0(2.2)	0.021842(14)	-0.53(28)	-10.(4)	0.001

TABLE VIII. Parameters for nonlinear fit beyond-TF LDA exchange data for alkali earths to Eq. eq:beyondTF. All rows $n \geq 10$ are included in fitting set. Blank spaces indicate where a parameter is held at zero. χ^2_{red} is reduced χ^2 measure, defined as the χ^2 error of the fit divided by the number of independent degrees of freedom in the fit set.

$\mathcal{A}$	$\mathcal{B}$	$\mathcal{C}$	$\delta\mathcal{C}$	$\mathcal{D}$	$\mathcal{E}$	$\chi^2_{red} \times 10^{-6}$
0.00833(12)		-0.0583(13)	0.0222(6)			5.1
	0.060(6)	-0.104(12)	0.0225(34)			180
0.00944(32)	-0.0087(24)	-0.0507(23)	0.0221(4)			2.6
0.00877(18)		-0.0656(27)	0.0220(5)	0.021(7)		3.2
	0.116(8)	-0.271(23)	0.0213(15)	0.32(4)		34
0.0097(5)		-0.096(14)	0.0224(5)		0.099(37)	3.5
0.0110(8)	-0.031(11)	-0.010(20)	0.02223(37)	-0.061(29)		2.0
0.0203(11)	-0.282(30)	0.70(8)	0.02220(14)	-0.68(7)	-0.71(8)	0.3

TABLE IX. Parameters for nonlinear fit beyond-TF LDA exchange data for alkali earths to Eq. eq:beyondTF. All rows $n \geq 2$ are included in fitting set. Blank spaces indicate where a parameter is held at zero. χ^2_{red} is reduced χ^2 measure, defined as the χ^2 error of the fit divided by the number of independent degrees of freedom in the fit set.